International Journal of Thermofluids 20 (2023) 100506

Contents lists available at ScienceDirect

International Journal of Thermofluids

journal homepage: www.elsevier.com/locate/ijtf

Cavitation analysis through CFD in industrial pumps: A review

Francesco Orlandi *, Luca Montorsi, Massimo Milani

DISMI - Department of Science and Methods for Engineering - University of Modena and Reggio Emilia, Reggio Emilia, Emilia Romagna, Italy

ARTICLE INFO

Keywords:
Cavitation
CFD
Pumps
Centrifugal pumps
External gear pumps
Mixed flow pumps
Axial flow pumps

ABSTRACT

Cavitation is one of the most detrimental fluid-dynamic anomalies that occur to turbomachines. It mainly affects machines characterized by high rotation speeds and clear distinctions between low and high pressure zones, where cavitation first appears. During the years, starting from the well known Rayleigh formulation for the formation of bubbles in a liquid medium, many models have been proposed to analyse the phenomenon. Spanning from higher simplifications to more detailed formulations, the range of applications of these models is wide and led to different quality results, where a clear methodology is not fully established when regarding specific sectors, for example the industrial pumps. Restricting the application field to few, specific kinds of pumps, i.e centrifugal, axial flow pumps, external gear and mixed flow pumps, this article analyses the main literature sources in order to give an overall view to the Computational Fluid Dynamic applications of the different cavitation models and their applications to industrial pumps.

1. Introduction

In various applications Computational Fluid Dynamic (CFD) has gained a vast use in order to simulate complex phenomena. The vast pump machine family, with its multiple ramifications, represents a new field where CFD is gaining more and more interest to be applied to. Since the physical phenomena that take occur in the working of these machines of an high complexity various methods have been used during the years. CFD is somehow the last approach and the higher in the precision of the results, but also the most challenging. Unfortunately it does not exist a single methodology to carry over a CFD simulation for these applications, mainly due to the intrinsic difference of the various machines, and this is an element of challenge itself. Also, it strongly depends on the single author of the simulation, also based on the software of choice. The available softwares are another world on their own. The main used are ANSYS FLUENT/CFX [1] and PumpLinx [2] which is mainly used for External Gear Pumps (EGP). Each software holds different methods to carry over the single simulations, where they differ fundamentally on the mesh management for the rotating and stationary domains in which the computational domain can be split into. Another important challenge is the complexity of the simulation regarding the physic precision. Obviously the more detailed the physic of the model and the harder to stabilize the simulation since less simplifications will hold. Also, in some cases critical physical events that are fundamental to the working of these machines cannot be simulated due to the inability of the numerical models to resolve it, and that is the case for the contact point of the EGP that is often neglected from the numerical simulation.

The last effort of the fluid dynamic simulations is the attempt to implement the multiphase models when CFD is applied to industrial pumps. Being characterized by two distinct phases, the working fluid (water, oil, etc.) and the trapped or coexisting air, the peculiar phenomena need to be analysed through two-phase numerical models as the Volume of Fluids (VOF) [3,4]. The high rotation velocities combined with peculiar operating or design conditions characteristic of a single machine often, if not always, lead to the formation of a vapour phase through the well known cavitation phenomenon. The simulation of this physic phenomenon represents a very important effort in the improving of industrial pumps since it is a very detrimental event. Not only the formation of vapour lowers dramatically the volumetric efficiency but it is also responsible for extensive wear of the components, leading to a shortage of the working life of the machine. The computational implementation of cavitation represents a step further to the correct modelling of pumps machinery. The choice of these then mainly depends on the software of use, since many of them implement native models or show a net preference for some over the others. It should be pointed out that a correct methodology should always consider cavitation models for pump machinery simulations. In peculiar and specific cases such as the contact point modelling, a peculiar bottle neck in the CFD simulations of EGP, not only the correct implementation of cavitation models is required but also the correct workflow of the machine is essential to the reliability of the results. This is the case for applications like gear pumps specifically. Also, and that depends much on the software of choice, the implementation of cavitation

* Corresponding author.
E-mail address: francesco.orlandi@unimore.it (F. Orlandi).

https://doi.org/10.1016/j.ijft.2023.100506
Received 19 July 2023; Received in revised form 28 September 2023; Accepted 28 October 2023
Available online 9 November 2023

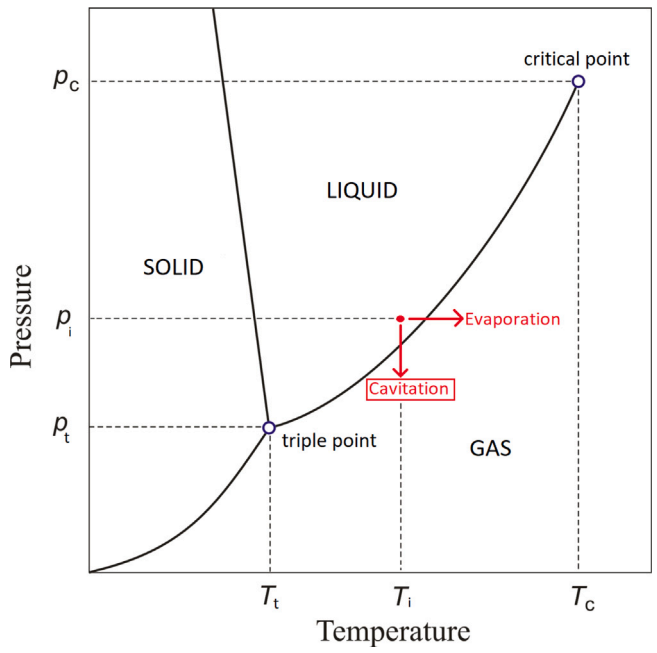

Fig. 1. Three phase graph for a generic fluid.

models and peculiar meshing techniques may boost the instabilities of the calculation, so that the simulation can be more prone to fail. In the present article a first glimpse in the concept of cavitation and its implementation in CFD techniques is given, restricting the analysis to the main models that are available nowadays. Then four kinds of industrial pumps are analysed through the given literature: centrifugal pumps, external gear pumps, axial flow pumps and mixed flow pumps. The results then will be discussed and summarized in the end in order to extrapolate an overall look upon the study of cavitation phenomenon in these field of application.

2. Cavitation phenomenon

By definition, cavitation is the phenomenon in which the formation of a vapour phase takes place in a fluid phase. This formation of the secondary gas phase can be originated by the fluid itself that converts into gas or from the liberation of previously dissolved gas into the fluid phase (aeration). In Fig. 1 a three phase graph for a generic fluid is shown. In the graph is shown that while the fluid itself is in liquid phase $f\left(p_i, T_i\right)$, where p_i is the pressure and T_i the temperature in that particular fluid point, two different iso-transformations are possible. With an isobar transformation, with the increasing of temperature T_i the fluid can change its state to the gas phase, where this transformation is commonly known as evaporation. If an isothermal transformation takes place, where the pressure p_i is sufficiently lowered enough, then the fluid can equally change its state to gas giving rise to the phenomenon called cavitation. It must be pointed out that this is possible only for temperatures over the triple point value, as shown in Fig. 1 In the case in which the formation of a gas phase interests eventual dissolved gasses the phenomenon takes the name of aeration.

Numerically, one of the first indicators that permits to value the tendency of a fluid to cavitate is the *cavitation number* defined as

$$C_a = \frac{p - p_v}{0.5\rho U^2} \tag{1}$$

where the difference $\left(p - p_v\right)$ represents the main cavitation rising factor, where p is the fluid reference pressure, p_v is the liquid vapour pressure and the denominator represents the dynamic pressure. It follows from Eq. (1) that lower the C_a the higher the fluid tendency to cavitate. Similarly to Eq. (1) in the field of turbo-machinery another quantity is generally of use since it is a fundamental characterization of all these kind of machines. This is the *Net Pressure Suction Head* (NPSH), which can be expressed as

- *Available NPSH* (*NPSHa*): the difference between the absolute pressure head and the vapour pressure of the working fluid

$$NPSH_a = \frac{p_{in} - p_v}{\rho_l g} \tag{2}$$

- *Required NPSH* (*NPSHr*): the head value at the suction side, namely the minimum pressure required to prevent the liquid to cavitate.

It is easy to understand, considering both C_a and NPSH, that the lower their values the higher the rising of cavitation. The use of such terms may be effectively able to reproduce an area where the secondary phase should appear, but in general this does not model the complicated and highly transient bubble growth and collapse process that characterize cavitation.

The vapour phase is governed by the vapour transport equation, which in its simplified form (neglecting the diffusive fluxes) appears as

$$\frac{\partial}{\partial t}\left(\alpha_v \rho_v\right) + \nabla \cdot \left(\alpha_v \rho_v \bar{v}_v\right) = R_e - R_c, \tag{3}$$

where α_v is the vapour volume fraction, while R_e e R_c represent the mass transfer rate of growing and collapse of the vapour bubble respectively.

Being the cavitation intrinsically dependent upon the initialization of a bubble growing from a solid surface it is necessary to define a so called seed-based model, where the seed represents a single nucleation site. With the initial hypothesis of spherical and uniformly distributed seeds in the surrounding liquid and an initial equal radius for each seed it is assumed that the number of seeds is proportional to the amount of liquid, so

$$N = n_0 \alpha_l V \tag{4}$$

where here is introduced the liquid volume fraction α_l, the liquid volume V and the number of seeds per unit volume of liquid n_0. The volume of vapour can be defined as $V_v = NV_b$, where the volume of a bubble is simply defined as $4/3\pi r_b^3$, so that the volumetric vapour fraction can be defined as

$$\alpha_v = \frac{V_v}{V} = \frac{4}{3}\pi r_b^3 n_0 \alpha_l \tag{5}$$

where when the volume fraction is known it is possible to obtain the local radius of bubbles as

$$r_b = \left(\frac{3\alpha_v}{4\pi n_0 \alpha_l}\right)^{1/3}. \tag{6}$$

From the definitions given above the next step is to make use of definition Eq. (6) in order to define the rate of production (or removal) of vapour which takes place in the vapour phase transport Eq. (3). Obviously, since the vapour bubbles move along with the flow, it can be approximately stated that the rate at which vapour is created corresponds at the rate at which the volume of the bubbles in the fluid is changing, leading to

$$\frac{dV_b}{dt} = 4\pi r_b^2 \frac{dr_b}{dt} = 4\pi r_b^2 v_r \tag{7}$$

where v_r is the bubble growth velocity. From Eq. (7) the rate of growth of all the bubbles in the fluid can be defined as

$$S_v = N\frac{dV_b}{dt} = 4\pi n_0 \left(1 - \alpha_v\right) V r_b^2 v_r \tag{8}$$

where is important to state that Eq. (7) refers only to the contribution of cavitation (indeed the vapour phase may derive also from boiling). If the vapour volume is rewritten in terms of the bubbles, considering

them to all have the same radius R and taking in account the number density of seeds n_0, the definition of $V_v = n_0 V_l 4/3\pi r_b^3$ is obtained so that Eq. (5) can be rewritten as

$$\alpha_v = \frac{n_0 \frac{4}{3}\pi r_b^3}{1 + n_0 \frac{4}{3}\pi r_b^3} \tag{9}$$

and from Eq. (9) it can be subsequently obtained a new expression for Eq. (6) so that

$$r_b = \frac{\alpha_v}{n_0 \frac{4}{3}\pi \left(1 - \alpha_v\right)} \tag{10}$$

so that finally the mass transfer rate per unit volume can be written as

$$R = n_0 \alpha_l 4\pi \rho_v r_b^2 v_r. \tag{11}$$

In Eq. (11) the only unknown is represented by v_r that is the rate at which the bubble radius changes. During the years various different models have been proposed where the aim is alternatively the definition of v_r (as happens for Rayleigh–Plesset or Schnerr–Sauer models) or directly R (as for Singhal or Zwart–Gerber–Belamri).

2.1. Rayleigh-plesset

As a starting point for all the most used models that have been proposed in the years the *Rayleigh–Plesset* equation is the most known. This is the equation that rules the dynamic of growing or collapsing of a vapour bubble. In its most known formulation it is written as

$$R\frac{d^2R}{dt^2} + \frac{3}{2}\left(\frac{dR}{dt}\right)^2 + \frac{4\nu_L}{R}\frac{dR}{dt} + \frac{2\sigma}{\rho_L r} + \frac{\Delta p(t)}{\rho_L} = 0, \tag{12}$$

where ρ_L is the surrounding liquid density assumed constant, $R(t)$ is the radius of the bubble, ν_L is the surrounding kinematic viscosity assumed constant, σ is the bubble-liquid interface surface tension, $\Delta P(t)$ is the difference between the external pressure at an infinite distance from the bubble and the bubble pressure, and is defined as $P_\infty(t) - P_B(t)$. In the formulation originally proposed by Lord Rayleigh [5], obtained from the spheric symmetry version of Navier–Stokes equation, the viscosity, superficial tension and non constant external pression contributions were not considered. The formulation that is used nowadays was defined by Plesset [6], but in general the most used in the vast majority of models is the simplified Rayleigh formulation

$$\frac{dR}{dt} = \frac{2}{3}\sqrt{\frac{p(R) - p_\infty}{\rho_L}}. \tag{13}$$

Eq. (13) represents the simplest form to describe the cavitation phenomenon. Here the rising of a vapour phase is described via the mechanic expansion of the gas bubble, which depends on the difference between the internal pressure and the surrounding. This formulation leads to an unrealistic development of the bubble due to the neglecting of the other terms, but is sufficient to first estimate the phenomenon. Over the years many models have been proposed that predict more or less precisely all the physics phenomenon that occur. As a general starting point and reference model for the other models, the **Full Rayleigh–Plesset** is based on Eq. (12), and is obviously the most expensive in terms of computational resources.

2.2. Schnerr-Sauer

The **Schnerr–Sauer** (S-S) [7–9] model is based on the hypothesis of an homogeneous mixture, and in order to avoid density distribution discontinuities it was conceived specifically to be coupled along with the VOF multiphase method. Starting from the VOF methodology the void fraction is modified as

$$\alpha = \frac{N_b \frac{4}{3}\pi R^3}{V_v + V_l} = \frac{n_0 V_l \frac{4}{3}\pi R^3}{n_0 V_l \frac{4}{3}\pi R^3 + V_l} = \frac{n_0}{1 + n_0 \frac{4}{3}\pi R^3}\frac{d}{dt}\left(\frac{4}{3}\pi R^3\right), \tag{14}$$

where n_0 is the nuclei concentration per volume unit of sole liquid and R is the radius of the bubble.

Generally the VOF method relies on the formulation by Spalding [10] who suggested to use the non-conservative form for the continuity equation

$$\nabla \cdot \bar{u} = -\frac{1}{\rho}\frac{d\rho}{dt}, \tag{15}$$

but as a consequence of the bubbles grow process it is no more divergence free and transforms in

$$\nabla \cdot \bar{u} = -\frac{\rho_v - \rho_l}{\alpha\rho_v + (1+\alpha)\rho_l}\frac{d\alpha}{dt}, \tag{16}$$

and the void fraction equation Eq. (3) will have the source term to the right defined as Eq. (14) so that

$$\frac{d\alpha}{dt} + \frac{\partial(\alpha u)}{\partial x} + \frac{\partial(\alpha v)}{\partial y} = \frac{n_0}{1 + n_0 \frac{4}{3}\pi R^3}\frac{d}{dt}\left(\frac{4}{3}\pi R^3\right). \tag{17}$$

So that the production of vapour phase is defined as the product between the bubble number (first term) and the volume change (second term). In this way the change of the cell vapour fraction does depend on the production of the vapour phase and the convective transport. Finally the relation to model the bubble growth is based on the hypothesis of no bubble-bubble interaction and their form to remain spherical. So with means of the R-P equation Eq. (12) together with the energy equation gives

$$R\frac{d^2R}{dt^2} + \frac{3}{2}\left(\frac{dR}{dt}\right)^2 = \frac{p(R) - p_\infty}{\rho_l} - \frac{2\sigma}{\rho_l R} - 4\frac{\mu}{\rho_l R}\frac{dR}{dt}. \tag{18}$$

Then it can be obtained that the grow of the bubble radius can be defined as

$$\frac{dR}{dt} = \frac{\rho_v \rho_l}{\rho}\alpha(1-\alpha)\frac{3}{R_b}\sqrt{\frac{2}{3}\frac{p_v - p}{\rho_l}}, \tag{19}$$

where p_v is the vapour pressure inside the bubble, p the local fluid pressure (similarly to p_∞ of Eqs. (13) and (19)) and R_b is the bubble radius defined as $\left(\frac{\alpha}{1-\alpha}\frac{3}{4\pi}\frac{1}{n}\right)^{1/3}$.

Then, if the system pressure is low and the difference $p(R) - p_\infty$ is large the definition in Eq. (13) holds. So the *Schnerr–Sauer* is basically a combination of the VOF method with the addition of a relationship to estimate the vapour change due to bubble growth and collapse.

2.3. Zwart-Gerber-Belamri

Another model of interest frequently used is of exclusive usage in the commercial software ANSYS FLUENT and CFX, elaborated by the developers themselves. The model of **Zwart–Gerber–Belamri (ZGB)** [11], starts from the well known simplified Eq. (13) and defines the total interphase mass transfer as

$$R = n\left(4\pi R_b^2 \rho_v \frac{dR_b}{dt}\right), \tag{20}$$

where n is the bubble density number. Defining the volumetric vapour fraction as

$$\alpha = N_b V_b = \frac{4}{3}\pi R_b^2 N_b, \tag{21}$$

where N_b is the bubble number per volume unit, substituting the definition of Eq. (20) it is obtained

$$R = \frac{3\alpha\rho_v}{R_b}\sqrt{\frac{2}{3}\frac{p_b - p}{\rho_l}}. \tag{22}$$

Being this formulation developed for the evaporative phenomenon as general formulation, it can be applied to the condensation phenomenon too, modified as follows

$$R = F\frac{3\alpha\rho_v}{R_b}\sqrt{\frac{2}{3}\frac{|p_b - p|}{\rho_l}}sign\left(p_b - p\right), \tag{23}$$

where F is an empiric coefficient with a value of 50 for evaporation and 0.01 for condensation. Given the initial assumption that bubbles do not interact with each other, valid only in the first instances of development, this invalidates the results reliability for the evaporation formulation, which is then valid for the condensation. The authors resolved this apparent limit by considering that with the increasing of the volumetric fraction has to correspond an increasing in density in the nucleation sites, substituting α with $\alpha_{nuc}\left(1-\alpha_v\right)$, where α_{nuc} is the nucleation sites volumetric fraction and α_v is the vapour volumetric fraction. This permits to rewrite

$$R=\begin{cases} F_{vap}\dfrac{3\alpha_{nuc}\left(1-\alpha_v\right)\rho_v}{R_b}\sqrt{\dfrac{2}{3}\dfrac{p_v-p}{\rho_l}} & p<p_v \\ F_{cond}\dfrac{3\alpha_v\rho_v}{R_b}\sqrt{\dfrac{2}{3}\dfrac{p-p_v}{\rho_l}} & p>p_v \end{cases}$$

where $R_b = 1e-6m$, $\alpha_{nuc} = 5e-4$. In the case of turbulent fluxes an additional modification is required to improve the resolving capacity of the flux oscillations with means of a reformulation of the turbulent viscosity as

$$\mu_t m = \rho_m C_\mu \frac{\kappa^2}{\varepsilon} = f(\rho) C_\mu \frac{\kappa^2}{\varepsilon}, \tag{24}$$

where

$$f(\rho) = \rho_v + \left(\frac{\rho_v-\rho_m}{\rho_v-\rho_l}\right)^n \left(\rho_l-\rho_v\right), \tag{25}$$

where the subscript "m" indicates the mixture.

This model then presents as its main peculiarity and characteristic the definition of the mass transfer due to cavitation, which acts as source and sink terms in the liquid and vapour continuity equations.

2.4. Singhal (full cavitation model)

In the **Singhal** model [12], known also as the *Full Cavitation Model*, all first-order effects are considered, as the formation and transport of vapour bubbles, the turbulent fluctuations of pressure and velocity and the magnitude of noncondensible gases. The starting point derives from an EVET (equal-velocity-equal-temperature) homogeneous approach, with the sequent hypothesis

- In the low pressure regions, where the cavitation phenomenon mainly happens and where high velocities are found, phase slip velocities are small enough to justify their neglecting.
- Bubbles generally are characterized by sufficiently small dimensions so that a more rigorous biphase simulation would end in an higher expense of computational resources compared to a not so better resolution.

starting from a vapour mass fraction defined as

$$\frac{1}{\rho} = \frac{f_v}{\rho_v} + \frac{f_g}{\rho_g} + \frac{1-f-v-f_g}{\rho_l}, \tag{26}$$

where with g are defined the incondensable possibly enclosed in the operative fluid mixture, with $\rho_g = WP/RT$ the incondensable density and $\alpha_g = f_g(\rho/\rho_g)$. In order to obtain the interphase mass transfer rate, continuity equations for the phases are defined

$$\frac{\partial}{\partial t}\left[\left(1-\alpha\right)\rho_l\right] + \nabla\cdot\left[\left(1-\alpha\right)\rho_l\overline{v}\right] = -R \tag{27}$$

$$\frac{\partial}{\partial t}\left(\alpha\rho_v\right) + \nabla\cdot\left(\alpha\rho_v\overline{v}\right) = R \tag{28}$$

$$\frac{\partial}{\partial t}\rho + \nabla\cdot\overline{v} = 0 \tag{29}$$

where $R = R_e - R_c$ and ρ is the mixture density and α is the vapour fraction. The usage of these continuity equations permits to obtain a relation between density and vapour fraction so that

$$\frac{D\rho}{Dt} = -\left(\rho_l-\rho_v\right)\frac{D\alpha}{Dt}, \tag{30}$$

and considering the vapour fraction defined as

$$\alpha = n\frac{4}{3}\pi R_b^3, \tag{31}$$

which is as the product between the bubble density number and the bubble volume. Substituting the definition Eq. (31) in the relationship Eq. (30) it is obtained that

$$\frac{D\rho}{Dt} = -\left(\rho_l-\rho_v\right)(n4\pi)^{1/3}(3\alpha)^{2/3}\frac{DR_b}{Dt}. \tag{32}$$

From the relation previously obtained and making use of the Rayleigh Eq. (13) the expression for the interphase mass transfer rate is obtained

$$R = (n4\pi)^{1/3}(3\alpha)^{2/3}\frac{\rho_v\rho_l}{\rho}\left[\frac{2}{3}\left(\frac{P_b-P}{\rho_l}\right)\right]^{1/2}, \tag{33}$$

which is generally known as *Reduced Bubble Dynamics Formulation*. This is a first approximation that can be used for the condensation phenomenon also. In the absence of other methods for the evaluation of the unknown "n", Eq. (33) equation can be rewritten for the evaporative contribution as a function of the bubble radius R_b obtaining

$$R_e = \frac{3\alpha}{R_b}\frac{\rho_v\rho_l}{\rho}\left[\frac{2}{3}\frac{p_v-p}{\rho_l}\right]^{1/2}, \tag{34}$$

Considering that

- $R_b \to 0$ for $\alpha \to 0$
- the phase change rate for volume unit should be proportional to the donor phase volume fraction
- in the vast majority of two-phase cases the dependency on velocity is linear. A good approximation is to consider (for turbulent fluxes) a characteristic velocity proportional to $\sqrt{k}$, with k the turbulent kinetic energy

it is possible to obtain two different expressions for R_e and R_c (it is important to consider that incondensable are also taken in account) as

$$R_e = C_e\frac{V_c h}{\sigma}\rho_l\rho_v\left[\frac{2}{3}\frac{P_v-P}{\rho_l}\right]^{1/2}(1-f) \tag{35}$$

$$R_c = C_c\frac{V_c h}{\sigma}\rho_l\rho_l\left[\frac{2}{3}\frac{P-P_v}{\rho_l}\right]^{1/2} f \tag{36}$$

For the Singhal model the vapour transport equation Eq. (3) takes the following general form

$$\frac{\partial}{\partial t}(\rho f) + \nabla\cdot\left(\rho\overline{v}f\right) = \nabla\cdot(\Gamma\nabla f) + \left(R_e - R_c\right), \tag{37}$$

where the first right hand side term takes in consideration the events of diffusion in the system.

3. Centrifugal pumps

Centrifugal pumps are one of the main kind of pumps employed in the industry. As for the most of the pumps their application spans through industries, agriculture and domestic use. The main components of this pumps kind are the impeller and the volute casing. As shown in the scheme in Fig. 2, the impeller is constituted by the blades and their support. Here the working fluid is caught up and whirled tangentially and radially outward until it leaves through all circumferential parts of the impeller into the diffuser part of the casing. The volute casing then is the mentioned final channel leading to the external circuit. The fluid momentum is so increased passing between the rotating impeller blades. It then reaches the impeller exit zone where the fluid high velocity is converted in pressure increase overcoming the required head. The fluid is continuously suctioned by the vacuum that creates at the impeller eye due to the blades rotating motion. In Fig. 3(a) a visual simplification scheme is given for the cavitation process in centrifugal pumps, while in (b) an actual evidence is provided. Alexis et al. [13] reported in their review on centrifugal pumps the various causes for which cavitation may occur. Between those, the most interesting ones for CFD analyses are

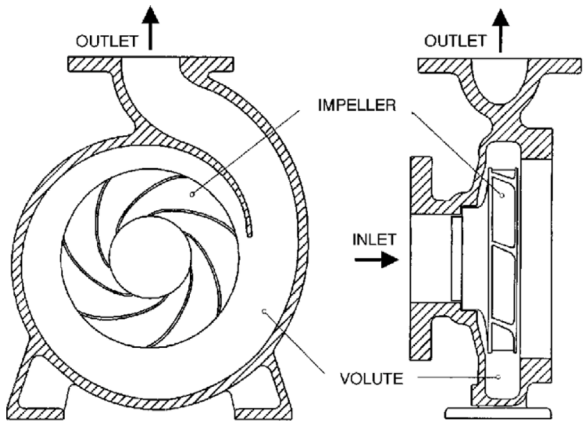

Fig. 2. Generic scheme for a Centrifugal Pump.

- Pressure drops due to flow area decrease.
- Turbulent fluctuations of the pressure field due to shearing between two neighbouring flows.
- Working fluid acceleration to the sharp edges that leads to pressure drops.

Considering the mechanical clear distinction between the components the CFD approach relies on the computational separation of the relative regions. Doing so two distinct computational regions are obtained that will be simply interfaced. One of the most used approaches is the Multiple Reference Frame methodology. Herein the volute case is solved with means of an absolute reference frame while the impeller through a rotating reference frame, Coriolis and centrifugal forces included. In the case of a static simulation then the interfaced get the Frozen Rotor Interfaces name, then for the transient simulation the Transient Rotor Interfaces are used. Regarding to the softwares, today ANSYS represents the most used software when it comes for centrifugal pumps. A part from the reliable results obtained in the various studies, the dedicated use of meshing softwares as ICEM-CFD or TurboGrid (as the name suggest specifically developed for such machines) led to the predominance of ANYS in the CFD analysis of centrifugal pumps.

3.1. Evolution of cavitation

By the definition of the Rayleigh Eq. (12), or also by the reduced form in Eq. (13), it is simply exposed that the cavitation rising directly depends on the operating conditions of the environment in which it manifests. Focusing only on the simplified Rayleigh Eq. (13), the environment pressure $p_{\inf}$ is the first element in which the operating conditions of the system come into play. Then the addition of other terms leads to a more realistic dependence to the environment surroundings. In order to value the performance decrease when cavitation takes place is mandatory to compare a simple one-phase flow neglecting the cavitation formation with the same case but with the addition of the vapour transport equation and a cavitation model in order to estimate the decrease in the parameters of interest. With means of a *Singhal* model Li et al. [14] described a detailed evolution of the cavitation validating the necessity to making use of an unsteady approach. That because the link between turbulence and vortices and cavitation development cannot be neglected. From this derives the main contribution to the head loss being the failing of the impeller to convert the kinetic energy into potential energy due to the presence of vortices and cavitation formation blocking the blade channel. Liu et al. [15] then, with means of a *Schnerr–Sauer* model, monitored the evolution of cavitation by means of the cavitation number in the range 0.150–0.036. The authors also found a mismatch between the experimental and simulated data regarding the NPSH evolution. Such difference in results is addressed to the friction losses and imperfections of the CFD code herein used (ANSYS CFX). Rehman et al. [16] operated an analysis of the inception of cavitation by means of a modified NPSH where the difference at the numerator is expressed as $p_{01} - p_{min}$. Here the first term is the upstream total pressure at the inception of cavitation and the second term is the minimum pressure at the downstream of the domain. The evolution of the bubble length was then linked with the NPSH values. For example, at NPSH equal to 20.023 m attached cavitation starts with a bubble length on blade surface less than or equal to the chord length, and no significant pump head drop is noticed. Lei et al. [17] focused on the pressure fluctuations happening in a centrifugal pump and investigated the rising of cavitation for partial discharge and large discharge. The amplitude of the pressure fluctuations was found to be higher when cavitation occurs, and then the evolution of cavitation with the decreasing of the NPSHa was found out. Specifically, the authors showed that the first apparition of cavitation is located at the leading edge of the blade suction side, while for several blades cavitation covers only half of the leading edge of the impeller hub. Then, once the flow enters the impeller a sharp turn of the flow passage close to the leading edge of the blade suction side appears that induces cavitation. Cavitation starts then to expand in the middle suction side, characterized by an asymmetric structure due to the asymmetric pressure distribution due to the interaction between the impeller and the volute tongue.

More recently, Tao et al. [18] analysed the evolution of cavitation for a reversible pump turbine in pump mode making use of the cavitation number. Firstly two different best ranges of values for best inception range and best critical cavitation range were identified, both based on specific values of the flow rate coefficient C_{ϕ}. Secondly an investigation was carried over for the inception of cavitation in pump mode, which was found to be dependent on the flow strike and separation in proximity to the blade leading edge. Here inception takes place in the leading edge pressure-drop region as shown in Fig. 4. At partial load conditions the fluid strikes on the blade pressure side and separation and pressure-drop happen on the suction side of the blade. At overload, fluid strikes on the blade suction, separation and pressure-drop then occur on the blade pressure side. The cavitation evolution is herein divided in 3 stages. The first stage is characterized with a small vapour volume fraction with a slow increasing after the inception of cavitation. The second stage is characterized by a quicker increasing with small-scale cavitation bubbles occurring in the impeller with a slight head increase. Finally in the third stage the increasing becomes very quick and large-scale cavitation bubbles occur in the impeller blocking the blade passage followed by a sudden decrease of the head to the critical standard. Cui et al. [20], with means of a *ZGB* model, then investigated the impact of an inducer, which is typically put to the upstream of the impeller in order to prevent severe cavitation. With an high degree of precision the different kind of possible cavitation where found and characterized with means of the cavitation number, which was systematically decreased at the design flow rate with a good agreement with the experimental results, that preliminarily showed the evolution of cavitation in the inducer through the four stages of incipient, critical, developed and deteriorated cavitation. The first is found to be caused by a tip leakage vortex observed for a specific cavitation number. With the continuous decrease of the cavitation number the region of cavitation expands and in correspondence to the blade leading edge blade attached sheet cavitation and cloud cavitation appear. Then severe backflow cavitations appear upstream of the inducer where large cavity bubbles extend halfway along the inducer passage, but these do not spread in the inducer passage. Finally deteriorated cavitation appears where most cavity bubbles occupy the downstream region of the inducer and start to enter the channels of the impeller with subsequent decrease of the head. Also the presence of cavitation surge, which is a periodical phenomenon where the bubble region will grow and decrease in size continuously, was detected and compared to the visual experiments.

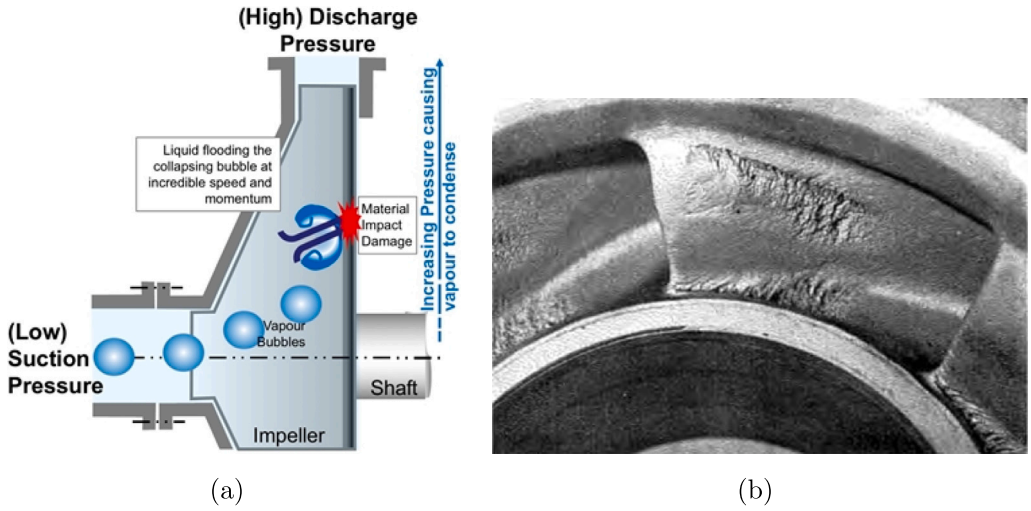

Fig. 3. (a) Diagram for cavitation mechanism in EGP by Flowserve. (b) Actual evidence of wearing on impeller blades due to cavitation.

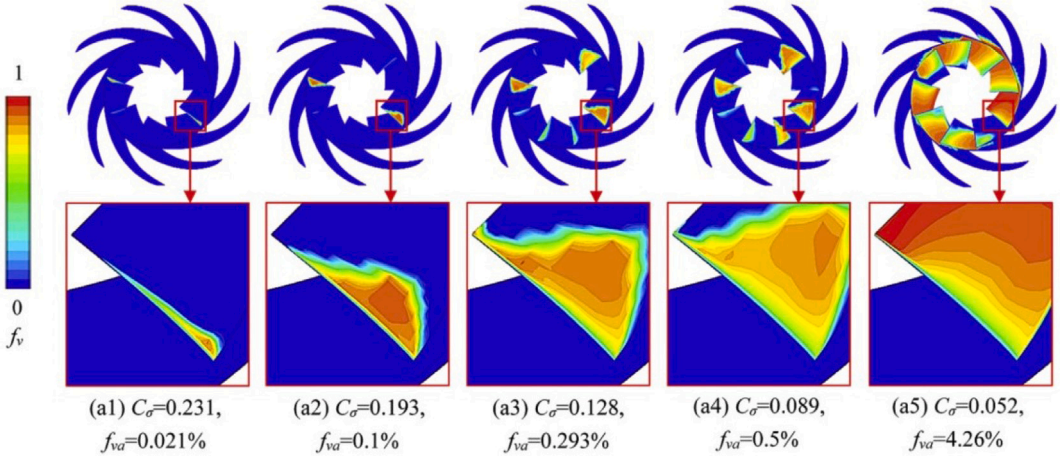

Fig. 4. Evolution of cavitation in Tao et al. [18].

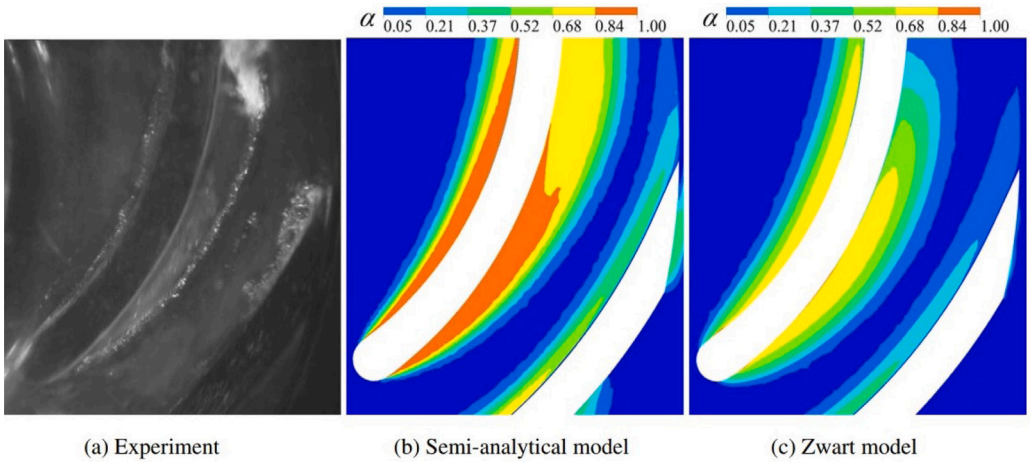

Fig. 5. Comparison of the results between the semi-analytical and the ZGB model for a given NPSH for a high speed camera frame in Ye et al. [19].

3.2. Existing models improvement

All the existing models are logically based on simplifying hypothesis, mainly upon the neglecting of the second orders terms. Then some authors proposed modifications to the existing models in order to improve the reliability of the results. Ye et al. [19] chose to use a semi-analytical model, which takes in account those second order terms that are most of the times neglected. This makes the model able to take in account the bubble-bubble interaction. The importance of this phenomenon depends on the inhibition promoted on the phase

change. This implementation then permits to predict the presence of large vapour zones. This model was compared to a standard *ZGB* model, which without the second order terms should overestimate the cavitation.

The authors demonstrated that for a wide range of NPSH, aside of the fact that due to the simplified geometry the discrepancy results in a small difference, that the *ZGB* model for bubbly cavitation overestimates the vapour volume fraction and underestimates the head, while the opposite happens for large cavities full of vapour as in Fig. 5. For the condensation phenomenon the *ZGB* model concentrates the main effect inside the cavity which results in a longer one at the pressure side. Lomakin et al. [21] demonstrated how the *Schnerr–Sauer* model is limited neglecting the surface tension term influence for the undissolved air presence case. This was demonstrated by the inclusion of the third phase that led to the increase of cavitation intensity after an increase of gas content. Pei et al. [22] formulated a new method to predict the NPSHr and consequently speed up calculation. This method makes use of custom boundary conditions by means of an algorithm that estimates a value for static pressure correlated to the 3% drop in the pump head. Similarly to the work by Ye et al. [19], Sun et al. [23] started from the *ZGB* model and proposed an improving by taking in account the bubble rotation. The bubble rotation permits to study cavitation-vortex pressure fluctuation interaction at partial loads, leading to an higher degree of precision. Cavitation is then divided in three stages: developing, shedding and collapsing cavitation. Two main vortex structures (characterized by different rotation verses) were found to be the promoters of the periodical shedding of cavities, with the development of cavitation that led to increase in the intensity of the vortices. This then led to the increase in the shedding. With means of the relative vorticity transport equation, with each component isolated to identify the single contribution, the authors found out that the relative vortex stretching term stretched effectively the cavity. Then the relative vortex dilation term promotes the cavity development. So, these two terms result to be the main contributors to the shedding phenomenon. Then cavitation instabilities have been found to be related to pressure fluctuations especially at cavity rear.

3.3. Operating conditions parametrization

There are two possibilities when cavitation is studied by means of parametric studies: the first makes use of varying the operating conditions while the machine dimensions remain the same, the second one changes the design parameter of the machine.

A way to find the cavitating conditions is to simply decrease progressively the inlet pressure until the requirements are met, as done in Li et al. [24], where a previous study (starting from a non-cavitating case) was validated by means of the *Schnerr–Sauer* model. Here a good agreement between cavitation number and head rise coefficient variation was met, and it was also found that until cavitation remained below 0.3 the head rise was unaffected, where the vapour generation appeared at the inlet side of the impeller. Muttalli et al. [25] characterized the cavitation (with means of pressure contour ranges) behaviour accordingly with the rise of the rotations per minute of the pump in exam, with the intermediate velocity of 8400 rpm being the one with the larger cavitation area developed. The results led to the conclusion that along with the rising of the mass flow following to the increasing velocity the subsequent rise in cavitation led to the decrease of the pump head. While not strictly an operating condition parametric study, the parameters employed in the cavitation models represent determined operating conditions. Then Liu et al. [26] investigated the influence of the *nucleation site radius* (NSR) which is employed in the term α_v in the first term of Eq. (20) of the *ZGB* model employed in ANSYS CFX and the two evaporation and condensation coefficients both appearing in . The authors showed that with smaller NSR the performances decreased subsequently to cavity region and length increasing, while the evaporation factor is found to regulate both region and length while the condensation has mainly effect on the regulation of the cavity length. Interestingly, results reach the best precision while cavitation covers all the suction side even if it should lead to a weakest ability to predict the correct results. Orcana et al. [27] linked the arising of cavitation to the fall of performance with decreasing of the charge height and pump capacity. In order to localize the cavitation phenomenon, pressure contour ranges were collected to individuate the portions where the conditions for the steam formation were reached.

Hu et al. [28] studied the cavitation occurring in a centrifugal pump tongue in overload conditions with means of a *ZGB* model. With the increasing flow rate the shedding of the separated vortices lowers the static pressure so that, coupled with the pressure fluctuations and shearing vortices derived from the flow separation, it will induce cavitation. In overload conditions then higher radical velocity and deviation of relative flow angle contribute to periodical variations of flow field near the tongue, which results in periodical cavitation evolution, with the frequency of cavitation cloud shedding being equal to the blade passing frequency (see Fig. 6).

The presence of cavitation at the tongue then was addressed to enhance the pressure fluctuations in the volute and also the blade loading distribution.

Xu et al. [30] used a *ZGB* model in order to investigate the effect of wall roughness by means of different smoothness values. The study lead to the result that wall roughness promotes cavitation in the impeller, also the low-pressure region in the impeller with the development of cavitation and further increased the vapour volume fraction on the blade surface as the flow loss. Zhu et al. [31] investigated the influence of leading-edge cavitation with means of *ZGB* model, and found that effectively in cavitation processes a variation in the impeller blade axial force was found. In the specific case the authors found an increase of 5% in the impeller blade axial force from no cavitation to small scales, and then a 13% decrease from small to large or even critical scales. Authors stated that cavitation on impeller blades strongly depends on local flow near impeller inlet and leading-edge. Then at partial loads flow separation and pressure drop is to be found mainly on the blade suction side. Then at design load these two phenomenons can be found on both suction side and pressure and then at over load are mainly located on the blade pressure side where a quick evolution is to be addressed to flow diffusivity.

3.4. Design parametrization

Another kind of study can be performed by simply modifying relative dimensions of components and observing the relative impact of such modifications. Xie et al. [32] investigated the effect of the impeller width in a parametric study starting from an impeller of 3 mm and then with 5 other smaller widths, with a following analysis on the relative NPSH. The analysis (unfortunately no model is herein mentioned) reported that the cavitation that appears in the back of the blade inlet reduces with the reduction of the width (Fig. 7), and an eventual reducing of the slot angle is capable of a further reduction of the vapour volume fraction. The same trend is more remarkably shown with an operative pressure of 50 kPa in respect to the previous 101 325 Pa. The results showed that a correct choice of the slotted impeller is able to redistribute the pressure along the impeller thus controlling the cavitation phenomenon.

Al-Obaidi et al. [33] with means of a *Schnerr–Sauer* investigated the correspondence between the number of blades of the impeller and the occurrence of cavitation. They found that with an increasing number of blades cavitation itself increases. Also, the starting point of cavitation is found to be located at the inlet eye of the impeller close to the leading blade. In another study Hu et al. [29] studied the influence of different inlet attack angles on the rise of cavitation. They found out that the incipient positions of cavitation remained nearly the same for all angles, while the most complicated flow structures found belonged to the developed cavitation where re-entrant jets were found in the cavitation zone, modelled with means of a *ZGB* model.

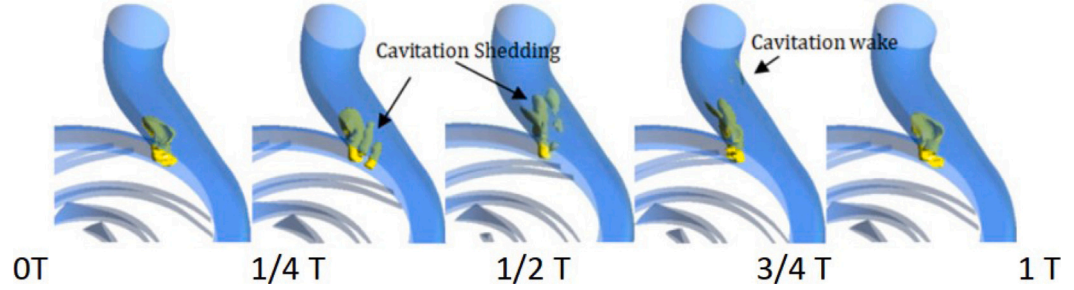

Fig. 6. Cavitation phenomenon at the tongue (for increasing spindle torque) in Hu et al. [29].

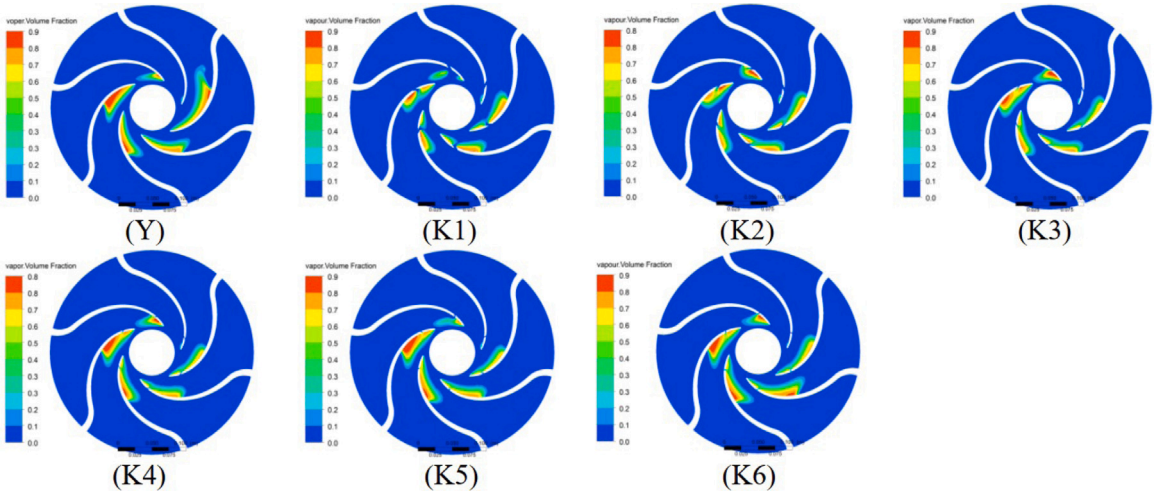

Fig. 7. Volume Fraction of vapour for the different widths of the impeller in Xie et al. [32].

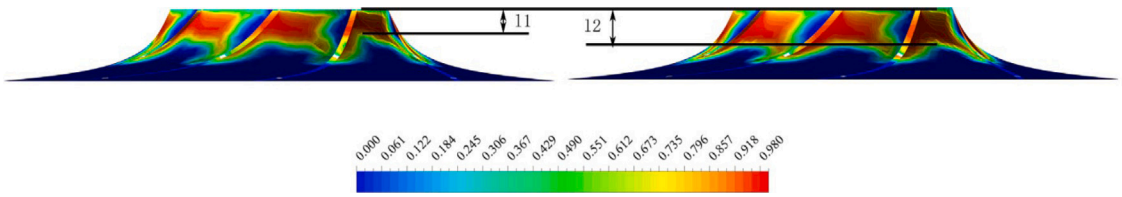

Fig. 8. Comparison of the vapour Volume Fraction for water (left) and Diesel (right) in Deng et al. [34].

3.5. Comparisons

Cavitation itself is obviously dependent to the liquid properties, so a comparison between different liquid in their tendency of being subjected to cavitation was operated by Deng et al. [34], where diesel and water where used. Also, the effects of viscosity and surface tensions were taken in account with means of an improved cavitation model based on a *ZGB* one. Diesel results to be characterized by larger areas of cavitation than water, as in the impeller region, as Fig. 8 shows. Effectively, regarding the 3D distribution water cavitation results higher in values but thinner, which means that is characterized by lower areas with higher vapour volume fractions. As the authors pointed out, the effect of the viscosity leads to the overall decrease of energy while surface tension will speed up the compression process and slow down the bubble expansion process, so that in diesel, where the viscosity is lower but the surface tension is higher, bubbles will change slowly so that larger areas with less vapour volume fractions are found.

Debarpan et al. [35] studied a centrifugal pump inducer with means of a comparison between the *Schnerr–Sauer* and the *ZGB* models. While no great difference is appreciable in the results, where both models reach a good agreement with the experimental data as in Fig. 9. The analysis showed that the inducer can effectively increase the head which prevents cavitation to take place, preserving for all the design points. The effectiveness of the inducer was demonstrated also in high saturation pressure conditions. In the case of Fecser et al. [36] the *Singhal* and *Schnerr–Sauer* models where compared with same operative conditions. Even if it should be a more accurate model, the Singhal model resulted in the less capable to reproduces the experimental results, with larger differences in respect to those elaborated by the *Schnerr–Sauer*. Unfortunately the motivations were not investigated but the results gave an interesting cue for further comparative analysis based on different cavitation models.

3.6. Adimensional parametrization

Shim et al. [37] characterized the cavitation by means of the simplified *Rayleigh–Plesset* equation and parameterized it with the use of a constant K_s which derives from the definition of the circumferential velocity at the volume inlet, namely $C_\theta = K_s(2gH)^{0.5}$. With the increasing of K_s asymmetric cavities started to form earlier in respect to the cavitation number. Also, using a flowrate near the best efficient point it was confirmed that cavities in the impeller are important for the reduction of the total head. When the flowrate was larger than the one of the best efficient point, then the total head reduction was determined

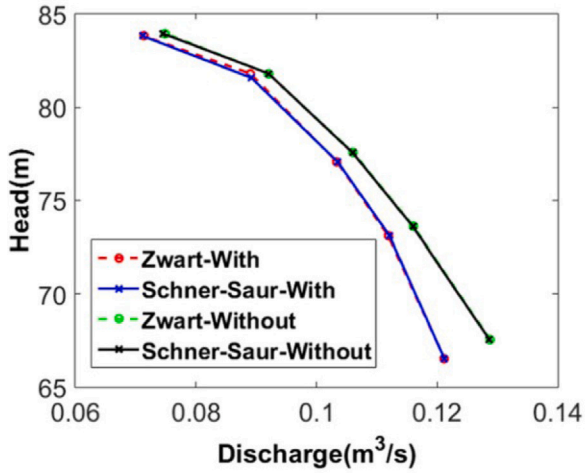

Fig. 9. Comparison through the Schnerr–Sauer and the ZGB models in Debarpan et al. [35].

mainly by the pressure loss near the volute diffuser. Thus suggests that the impeller and the volute geometry are important factors in the rise of cavitation.

4. Axial flow pumps

An axial flow pump is a type of centrifugal pump in which the fluid enters and exits the pumps in a parallel direction to the impeller (see Fig. 10). So an axial flow pump does not change the flow direction of the working fluid differently from a centrifugal pump. This is obtained by the design of the blades so that the pump discharges the fluid axially in a parallel direction to the impeller, which is parallel to the suction. For the similarity with the ships' propellers this kind of pumps is sometimes called as propeller pumps. They are generally employed when low head and high flow rates supplies are required, such as marined industries, sailing ballast, water pumping, sewage treatment, pump bilge and so on. In the axial flow pump the impeller blades guide the fluid axially, and the pressure generates by the fluid passing over the impeller vanes. The impeller blades have an airfoil section through which the fluid runs and leads to the generation of pressure. The liquid is forced in the direction of the rotation axis of the impeller, and that is why the fluid particles do not change their radial position as flowing through the pump. The cavitation phenomenon then, considering the above brief description, is mainly located in the space between the impeller blades and the guide vane. With the lack of summary reviews on the argument, as far the authors know, the work of Xi et al. [38] will here be used as a reference to experimental verification of cavitation in the axial flow pumps. In their study the tip leakage vortex and the induced suction-side-perpendicular cavitating vortices were investigated in multi-operating conditions. Also, the pressure fluctuations where investigated to clarify the relationship between the pressure field and the tip cavitation. In the extensive analysis the authors found out that

- With the decrease in pressure cavitation inception occurs earlier in respect to design and overload conditions.
- With the increasing flow the incipient position moves to the back edge of the blade chord.
- When the cavitation number decreases the triangular cloud cavitation area (formed in the blade tip) increases and the cavitation morphology becomes more unstable.
- Cavitation in the tip region is characterized as a low-pressure area, and the Tip Leakage Cavitation (TLV) cavitation appears as a narrow and long range of low pressure, when the pump operates at overload conditions.
- The TLV cavitation and blade tip are connected by the shear layer cavitation to form a triangular cloud cavitation as the flow rate and cavitation number decrease
- The unstable cavitation cloud have been found to have an effect on the pressure field.

In CFD analysis, since these pumps are fundamentally identical to the centrifugal pumps apart from the casing the numerical analysis follows more or less the same methodology as per the centrifugal pumps. This is generically found in the subdivision of the computational domain, where the interfaces methodology of the multiple reference frame is often applied, i.e. dividing the static blades from the rotating ones regions. The same applies on the reference software, where for the vast majority of published articles ANSYS (being it in the CFX or the FLUENT suites) results in the prime choice for the analysis of these machines.

4.1. Operating conditions

As for the centrifugal pumps a simple way to simulate an axial flow pump is the investigation of the different response to a variation of the operating conditions. Ding et al. [39] in their study proved the efficiency of Pumplinx in the analysis of various machines, in which one was an axial flow pump. By the use of the *Singhal* cavitation model and the moving/sliding interfaces, where the rotating and stationary regions are treated separately and connected by the common interfaces, the authors characterized the cavitation in a single stage large vertical cooling water pump. In the analysed work various duty flows from 60% to 120% where considered. The authors showed clearly the small gap effect, where a cavitation region at the suction side of the impeller was reported, induced by strong cross flow over the tip gap. It was found that an MRF methodology (Moving Reference Frame) tends to slightly underestimate the pump head in respect to a fully transient methodology. The authors also characterized the bubbles dimension correlated to the duty flow. Finally a prediction was carried over regarding the incipient cavitation, resulting in a slight under-prediction in comparison with the tests results. Hosono et al. [40] investigated the mechanism of the pump head decrease along with the cavitation rising. The authors made use of ANSYS CFX and *R-P* model for cavitation modelling. The paper reported that with the decreasing NPSH (as it can happen with smaller machines characterized by higher speeds) the angular momentum increases even if it seems to be not linked to pressure and head coefficients changes. The high loss coefficient area due to the tip leakage and cross sectional flows in cavitating conditions increase. Then the authors stated that the changes in pump head due to cavitation are the result of the balance between the increasing angular momentum and the loss highlighted by changes in streamlines on the blade surface.

Shi et al. [41] studied the tip leakage vortex for an axial flow pump on the cavitation generation. In this paper the authors, with means of ANSYS CFX and *ZGB* model, studied different flow rates and the corresponding cavitation numbers. With means of a λ_2 vortex criterion the authors characterized the vorticity and pressure along the TLV trajectory, where a comparison with the experimental results are shown in Fig. 11. The vorticity decreasing and the pressure increasing in the vortex core was used as indicator for the emerging cavitation. This is characterized by three layers near the tip region and interact with the TLV. The cavitation tends then to appear earlier for small flow rates, mainly consisting of tip clearance cavitation. In the end an interesting phenomenon is that for which the cavitation increases the vortex intensity under slight cavitation conditions while it dramatically eliminates the TLV for low cavitation numbers. Shen et al. [42] investigated the tip leakage relation with cavitation in an axial pump for three different off-design conditions, with means of ANSYS CFX and the *ZGB* cavitation model. The authors obtained good matching results and furnished a detailed analysis of the cavitation phenomenon. In the

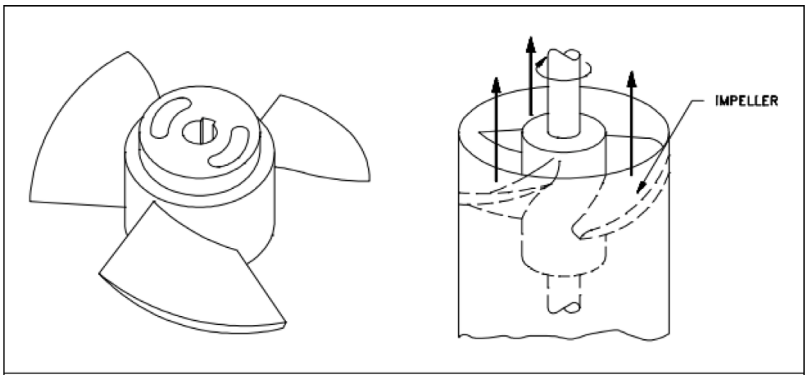

Fig. 10. Generic simplified scheme for an Axial Flow Pump.

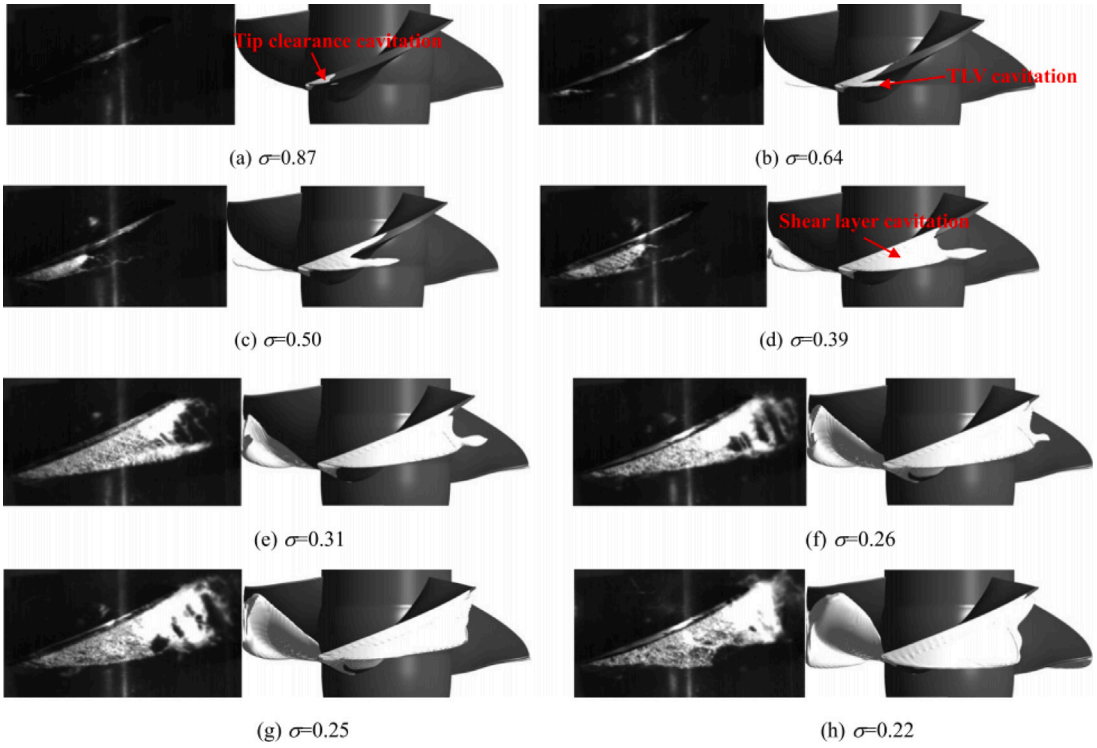

Fig. 11. Different cavitation patterns for a vapour fraction equal to 0.1 and different flow rates as reported in [41].

present work the cavitation in the tip clearance includes tip leakage vortex, shear layer, corner vortex and blowing vortex cavitation. The sheet cavity then attaches to the blade surface. With the reaching of severe cavitating conditions hub cavitation also appears. Also, the flow passage is found to be blocked with the migration of shedding cavitation, and the cavitation flow field resulted effectively influenced by the flow rate.

4.2. Design modifications

Along with the operating conditions investigation, as explained also for the centrifugal pumps, the variation in design characteristics is a common research topic. Li et al. [43] analysed two different axial flow pump impellers, where one (A) was the reference one with constant circulation at outlet while the other (B) was an optimized one with variable circulation. With means of FLUENT and the use of multiple reference frames for the rotating effect of the fluid the calculation was firstly used to characterize the two different impellers performances. Then a non-better specified FLUENT cavitation model (most probably being the ANSYS exclusive *ZGB* model) was used to evaluate the cavitation on the impeller blades. The result showed that compared to impeller B, NPSHr in impeller A was not only substantially higher but also declined much more rapidly with reducing NPSH. Comparing the vapour fraction contours reported for the impeller A and B the authors declared that the suction performance of impeller A was poorer than that of the impeller B. The authors nonetheless pointed out that for such simulations two limitations were reported, namely the approximated effect of suction entry of the flow (simplified in this case with a free-vortex and uniform axial velocity) and the neglecting of the effect of diffusing component behind the impeller. Cao et al. [44] proposed the analysis of an axial pump characterized by a contra-rotating rotor with means of ANSYS CFX and transient rotor–stator model. The authors started by an RR2 design based on the NACA4 models. Then three different models of the new RR3 design where analysed, with a combination of integrated or free vortex inflow velocity model and variable or consistence maximum camber location. The authors made use of the NPSH calculation to determine the design rotational speed. In this study is analysed the possibility of cavitation in terms of cavitation inception with the minimum pressure obtained by single-phase transient simulations, so no effective cavitation model

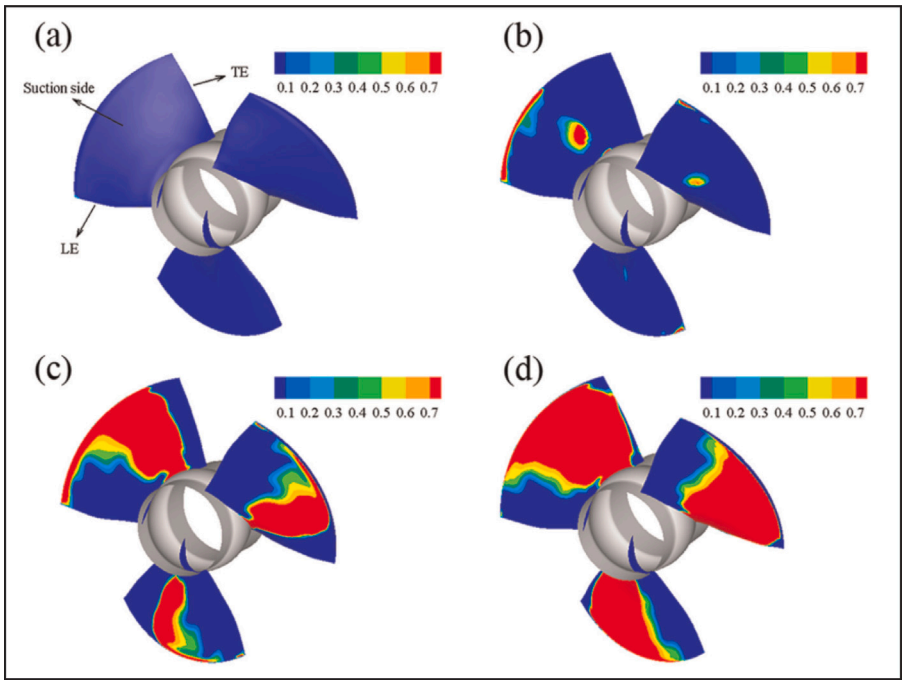

Fig. 12. Volume fraction of vapour around the blade suction side under different design points in [45].

is herein used. The new model resulted in an improved cavitation inception performance. This was expected by the authors, even if no superiority in the cavitation inception was shown, for the cavitation on the blade surface was expected to develop much slower than the starting design. Also, the blade optimization is said to also be able to limit the cavitation development to the suction surface. Feng et al. [45] studied the cavitation performance of an axial flow pump for different flow rates with the addition of inlet guide vanes. The numerical method included the ZGB cavitation model and the multiple reference frame in ANSYS FLUENT environment. The investigated IGV angles were chosen as −10°, 0° and 10°. Linked to the different flow rates the authors proved that the cavitation performance of an axial flow pump can be improved with positive IGV angle values for low flow rates and with negative IGV angle values for high flow rates. The authors also found out that the connection between the cavitation zone from the tip side close to the leap edge and the cavitation zone from the hub part of the suction side is an important signal to indicate the great deterioration of pump performance. An example of the prediction of the cavitation at different design points is shown in Fig. 12.

Inherently the analysis of a screw axial flow pump Lin et al. [46] studied the influence of three different tip leakages on key parameters and cavitation. The authors used ANSYS CFX, *ZGB* cavitation model and the frozen rotor interface between the rotating and the stationary regions. The authors found out that with increasing tip leakages the vorticity distribution in the impeller gradually spreads from the hub to the tip of the blade inlet. On cavitation, the increasing tip leakage leads to a decreasing of the NPSH and an increase of the critical NPSHc that leads to earlier apparition of the vapour phase. For this kind of machine the development of cavitation resulted limited to the inlet of the blade suction-side near the hub for incipient cavitation. The blade suction-side surface then is quasi entirely submerged by the vapour phase when the cavitation number reaches the fracture cavitation state. Following up the previous paper in the same year Shi et al. [47] studied the effect of different blade tip geometries on the TLV dynamics and cavitation patterns for an axial flow pump. Using ANSYS CFX and the ZGB cavitation model the authors investigated a first shape edges clearance (plain tip), a second rounded edge on the pressure side and a sharp edge on the suction side (rounded tip) and a third one with flat edge on the pressure side but the gap height diverged slightly towards the suction side (chamfered). First the performances are worsened by the rounded tip (attributed to the tip leakage vortex) while the chamfered tip presents the highest performances. The main advantage of the round tip is the elimination of the tip separation vortex making the flow more homogeneous in the clearance. Regarding the cavitation phenomenon then the tip clearance cavitation is dramatically eliminated by the absence of tip separation vortex. In the case of chamfered tip the cavitation is more intense in consequence of the tip clearance vortex with high TLV. This effect is clearly visible in the reported cavitation patterns. Xu et al. [48] investigated the tip clearance effect on a scaling axial flow pump. The authors made use of ANSYS CFX and investigated the vortex structures with a focus on the TLV, comparing them the results with the experimental cavitation patterns. Doing so two main vortex structures where found which the dimension is directly dependent on the size of the tip leakage. The cavitation was found out to appear in the TLV of the axial flow pump. With different gaps the position and intensity of the TLV cavitation are different, and with the decrease of the cavitation number the size of the strength of TLV under tip clearance gradually increases.

4.3. Cavitation characterization

Another well analysed research topic on the axial flow pumps is the characterization of cavitation. By these is intended the detailed analysis of the evolution of the cavitation phenomenon, from its initial generation to the most critical operating conditions. Its further division into different cavitation levels depends on the authors and the capability of the methodology applied. Anyhow, the cavitation detailed analysis can be divided more or less in three main steps starting from the initial incipient cavitation to the most developed or critical cavitation. In their article from 2007 Saito et al. [49] proposed a numerical code to predict the cavitation development for a three blade axial pump and a cage-guided valve. The cavitation model therein integrated was the *Singhal* and its resolution, along with the Navier–Stokes system, was solved by applying a fractional step method. This way the authors divided the cavitation in the axial flow pump as inception cavitation and developed cavitation. The first was divided in three different bubble cavitations, being K1 the one happening in the forepart of the foil in a low flow

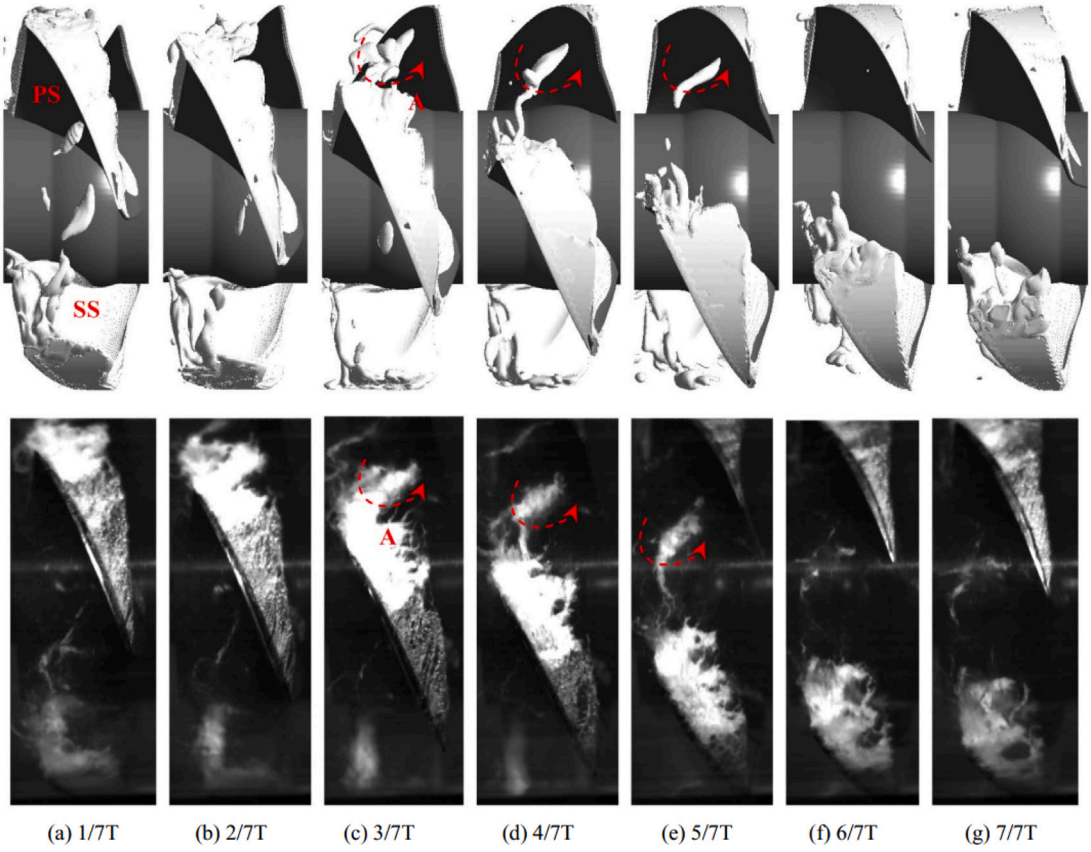

Fig. 13. Up: Time evolution of the three-dimensional cavitation patterns in the tip region and Down: Experimental side view of the TLV cavity in [51].

range, K3 happening in a middle flow range on a shoulder part of the suction surface and finally K2 for high flow rates and negative flow incidence, this being a sheet cavitation on the pressure surface near the leading edge. Zhang et al. [50] made use of the Boundary Vorticity Flux (BVF) to characterize the cavitation development in a slanted axial pump. This technique requires a previous simulation of the cavitation in the calculation environment, in this case ANSYS CFX with the *ZGB* cavitation model and frozen rotor interfaces, and then a successive investigation with the BVF to further investigate the flow patterns. The simulated cavitation for this axial pump showed, for different NPSH, the evolution from incipient, to critical to deep cavitation along a blade. First some cavities appear with the incipient cavitation at the leading edge, where the tip clearance cavitation enlarges linking to the vortex cavitation in critical cavitation conditions. Then with deep cavitation conditions the cavitation pattern becomes larger and isolated bubbles can be observed in the flow field. The BVF then, defined as composed by the surface accelerated speed, the pressure gradient and the boundary vorticity, showed that with the cavitation becoming deteriorating a larger recirculation on the blade suction side approaches the trailing edge and leads to the formation of the side-entrant jet. Then with critical and deep cavitation a prominent BVF emerges near the trailing edge.

In another study the same authors Zhang et al. [51] with ANSYS CFX and the *ZGB* cavitation model focused on the unsteady TLV cavitation, which is shown in Fig. 13. In order to further analyse the vortex structure an improved filter-based model that was obtained by modifying the eddy viscosity term, that in the RNG turbulence models tend to be over-predicted. The authors investigated then the instantaneous cavitating vortical flows, i.e. the vortices that are prone to cavitation under low pressures. The cavitation was then classified as tip clearance cavitation, shear layer cavitation, tip leakage vortex cavitation, sheet cavitation on the blade suction surface and shedding vortex cavitation at the blade trailing edge. Recalling on past studies of the same authors the tips leakage vortex core and the counter-rotating induced vortex near the end-wall where identified. Finally the authors concluded that at the sheet cavitation trailing edge in the blade tip the perpendicular cavitating vortices are induced by the TLV and then migrate towards the pressure side of the neighbours blade leading to severe degradation of the pump performance. As a new topic Wang et al. [52] investigated the evolution characteristic of the Suction Side Perpendicular Cavitating Vortex (SSPCV) in an axial flow pump with means of ANSYS CFX and the *ZGB* cavitation model and the transient rotor–stator interface. In order to correctly identify the SSPCV the authors made use of the Liutex vortex method which can eliminate the shear pollution on the wall and so facilitate the individuation of the desired vortex structure. Other methods employed are the vortex velocity gradient, vortex kinetic energy, and vorticity transport equation. The first as mentioned is useful in its ability to reduce the noise pollution but, due to the threshold, the characteristics of the SSPCV cannot be displayed. The vortex velocity gradient and the vortex kinetic energy can show the influence range of the vortex but since cavitation is also responsible of velocity gradients these methods are sensible to other factors. The latter then is the less intuitive and quantitative since it analyzes the origins of vorticity from the point of view of micelle, focusing on the internal mechanism of vortex. The results showed that the SSPCV is formed by the combined action of cloud cavitation shedding and tip leakage in the tip region, and its rotation direction is the same as that of the impeller. The evolution of SSPCV was divided in three different stages being formation, development, and breaking stage.

The effect of ambient pressure and inflow uniformity on the vortex and cavitation dynamics in an axial flow was investigated by Gong et al. [53] with means of Star-CCM+ and the *S-S* cavitation model. In Star-CCM+ the interfaces between the transient and static regions are basically solved as in the multi-reference frame. For the present

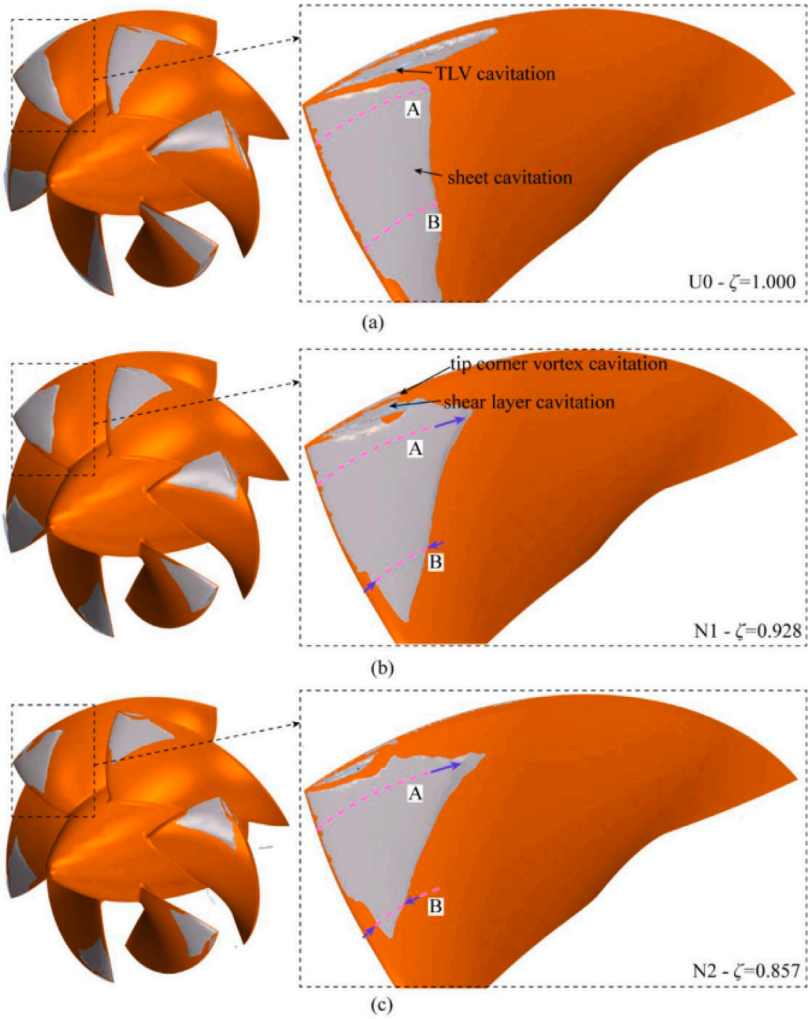

Fig. 14. Instantaneous cavitation morphology of the impeller blade for different flow uniformity ζ in [53].

work two non-uniform inflow conditions with different gradients were applied aside from the uniform velocity inlet condition. The two non-uniform conditions were defined with different values from the casing centre to the peripheral wall. The conclusions of the authors are that first the primary tip leakage vortex (PLTV) forms from the blade tip corner and extends to the pressure side of the adjacent blade as in Fig. 14. The primary and secondary TLV vortices happen to merge and the water-vapour interface tends to add instability to the vortices. The lower ambient pressure promotes the evolution of TLV and gives rise to larger vortex structures and faster energy dissipation in the flow passage. For cavitation the lower ambient pressure gives rise to higher instability with irregular interfaces near the closure region of the sheet cavitation. The vorticity transportation in the cavitating flow is dominated by the vortex stretching and dilatation. The axial non-uniform inflow alters the angle of attack of the airfoil at different radius of the impeller blade. Then this non-uniformity promotes also the merging between the preliminary and secondary TLV. The compression-expansion of the sheet cavitation occurs as for the vortices under the non-uniform condition.

4.4. Others

Feng et al. [54] proposed a new cavitation model to be applied to an axial flow pump. The declared aim of the authors is to enhance the cavitation prediction capability of the existing models. In order to accomplish the objective of the research the authors made use of ANSYS FLUENT's UDFs routine, and then compared the obtained results with a *S-S* cavitation model results. The newly proposed model is based on a truncated Rayleigh–Plesset equation. Pointing the fact that in the *S-S* model the vortex effects on the cavitation bubble radius are not taken in account (and as above the strong correlation between the vortex structures and the cavitation was sufficiently stressed), the authors used a new function F_r to implement the vortex-cavitation interaction effect. This function considers the factor of local vortex and is defined as $\frac{1}{2\pi} * |\Gamma|$, where $|\Gamma|$ is the circulation of vortex. In the computation of the F_r function the authors took in consideration the rotating function, the reference velocity scale, the characteristic length scale, the shear strain rate and the vorticity magnitude. The equation used as a starting point for the new model is a alternative truncated *R-P* equation which also considers the contribution of the second-order derivative of the general formulation Eq. (12), which is also neglected in the *S-S* model. This improved cavitation model was solved coupled with a turbulent filter-based density correction model (FBDCM) that implies the correction of the over-prediction of the turbulent eddy viscosity in the cavity enclosures and cavitating wake flows. The proposed model resulted more capable in predicting results closer to the experimental findings. The unsteadiness and turbulence of cavitation, as well as the 3D shape was captured, and the cavitation performance at three different flow rates were closer to the experiments in respect to the *S-S* results. The cavitation inception is therefore found out to firstly appear as the corner vortex cavitation in the tip clearance. After that the shear layer cavitation and TLV cavitation occurs. As a detail on the sheet cavitation

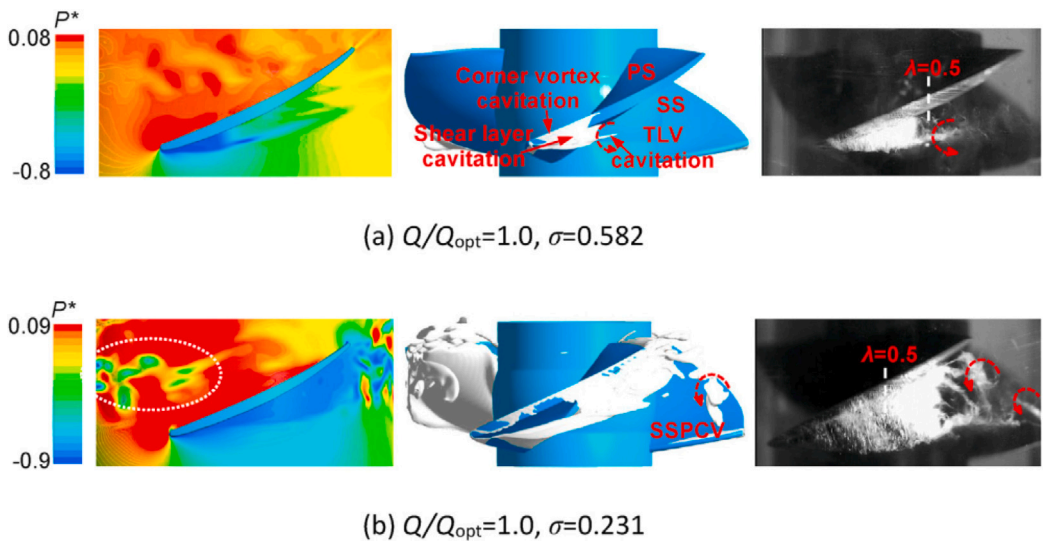

Fig. 15. Pressure field and corresponding cavitation in [55].

on the suction surface development, the authors found out that it firstly occurs at the leading edge near the blade tip then, with the decrease of the cavitation number, it develops towards the trailing edge and the hub together.

In their study from 2021 Xi et al. [55] analysed the induced effects of cavitation and TLV on the pressure fluctuations. A peculiarity of this study resided also in the turbulent model implemented (although no software is specifically named), which is the Detached Eddy Simulation, that combines the use of RANS equations in the near wall regions and then switch to the LES method in the detached regions. This gives an higher accuracy thus saving computational time in respect to a pure LES turbulent method. The calculations led to the discovery of obvious periodicity found in three peaks and three troughs in an impeller rotating revolution. This is attributed to the pressure difference between the suction side and the pressure side of the blade. The link between pressure and cavitation is then well shown in Fig. 15, where the pressure field, the cavitation vortices and the experimental results are compared. With decreasing cavitation numbers the periodicity becomes more clear and more evident with the decrease of the flow rate. The tip cavitation was found to be highly related to the cavitation number. The SSPCV generates from the trailing edge of the cavitation cloud and results in the collapse of the triangular area characteristic to this phenomenon. Then the evolution of the SSPCV was divided in three stages: Generating stage, Shedding stage and Dissipating stage.

4.5. Wear models

A new focus of interest in the axial flow pump CFD simulations is the use of wear models that can predict the migration and effect of particles present in the working fluid (as for draining applications). The presence of such particles leads to sediments and detrimental effects, mainly structural damages, on the impeller blades and so decreases dramatically the performances.

Lin et al. [56] investigated the joint effects of cavitation and sediment wear on an axial flow pump. Various parameters have been taken in account to study the trajectories and the sediment law of the particles, such as sediment concentration, particle size, and cavitation stage. The authors used ANSYS CFX, the *R-P* cavitation model and the wear model, that takes in count as main parameters the collision velocity and angle of the particles, the properties of the particles, and the material surface (in this case steel and aluminium). The formulation for the wear rate, i.e. the material mass worn by the particles acting on the per unit of the surface, namely E, is as follows

$$E = f(\theta)\left(\frac{V_p}{V_1}\right)^2 \cos^2\theta\left[1-\left(1-\frac{V_p}{V_3}\sin\theta\right)^2\right]+\frac{V_p}{V_2}\sin\theta$$

where θ is the particle collision angle, V_p the particle impact velocity, and V_1, V_2, V_3 are the particle collision velocity parameters. The results demonstrated the mutual worsening factor of cavitation in the presence of sediments. The cavitation increases the solid volume fraction and thus further accelerates the wear on components. As cavitation develops, the maximum wear rate increases while sediment concentration remains the same, thus indicating that cavitation accelerates the wear on the impeller surface. When cavitation worsens and the particle size remains the same, the maximum wear rate increases. Those results confirm that cavitation and wear are mutually worsening in a positive relationship. When sediment concentration is low cavitation remains the dominant damage factor but with the growing in concentration of solid particles wear becomes the first damage contributor. One effect of mutual worsening happens when the surface is subjected to sediment wear, so that the uneven surface will give rise to flow separation and vortex, which in turn exacerbates cavitation. Then the material of the flow surface becomes more fragile due to cavitation, which in turn exacerbates wear on the surface.

The same authors the next year [57] investigated the difference between clean water and sandy water separately as working fluids. Here ANSYS CFX and the *ZGB* cavitation model are employed (no effective explanation is given to the wear model, but it is supposed to be the same as for the previous work). The increase of sediment concentration leads to increasing in the blade vortex range and cavitation region and increases also the disorder of the flow pattern in the impeller, as in Fig. 16. This way is proven by the authors that sediments worsen the internal flow pattern in the pump, promotes the cavitation and reduces the cavitation performance of the pump. The influence of particle size is similar to the sediment dimension but the cavitation in sandy water is substantially different to that happening in clean water, with the first being larger than the second.

5. Gear pumps

Gear Pumps represent a large family of volumetric displacement machines, and as for the Centrifugal Pumps or Axial Flow Pumps the applications span widely in between of various areas of interest. Beside of the various existing typologies, the basic working principle is focused on the displacement of fluid by means of displacing volumes.

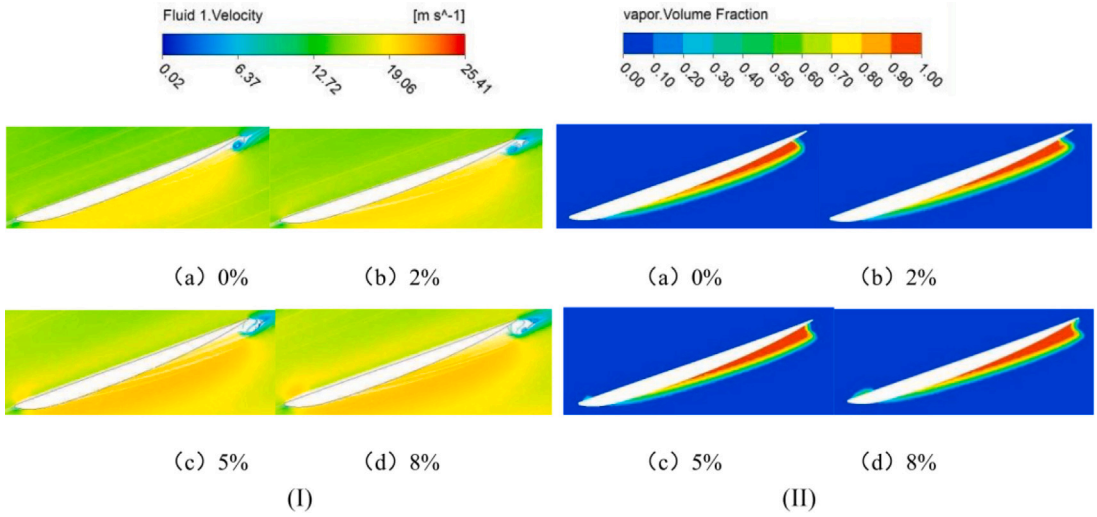

Fig. 16. Streamline and cavitation volume fraction distribution of the blade under different sediment concentration C_m in [57] (inlet pressure = 45 kPa): (I) streamline distribution and (II) cavitation volume fraction distribution.

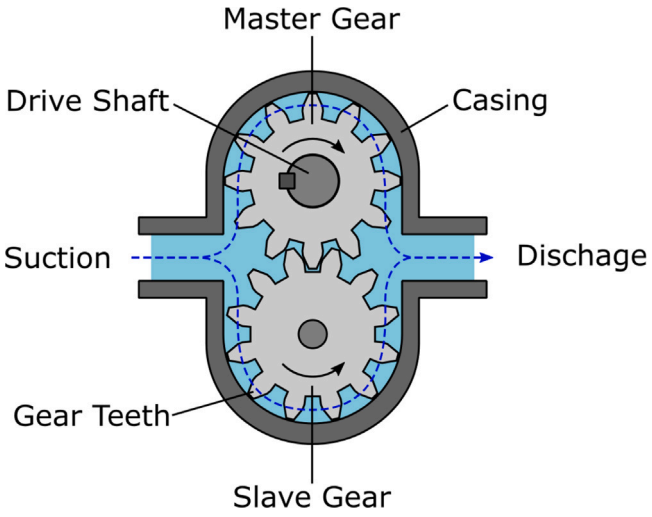

Fig. 17. Generic working scheme for an External Gear Pump.

These machines trap the fluid on the suction side and discharge it at a higher pressure on the discharge side. For External Gear Pumps, which working scheme is shown in Fig. 17, the fluid enters the pump on the suction side. The rotation of the gears (led by the driving gear, or master, to the driven gear, or slave) traps the fluid in volumes between the gears teeth along the peripheral casing. Then to the discharge side the volumes open and release the fluid which is moved out to the circuit due to a pressure gradient. Part of the fluid is then trapped in a closed volume which is generated after the mating of the teeth in the middle section of the pump. Once this volume opens to the suction side the sudden pressure fall leads to the release of the trapped air (aeration) or generation of working fluid vapour. An exemplary frame is reported in Fig. 18 where the contact point is visible on the right, while on the left is clearly visible the secondary phase propagation to the suction side with the opening of the fluid pocket.

The aeration/cavitation phenomenon here depends on the effective mechanic separation of the suction and discharge regions. This separation, which is necessary for the volumetric efficiency of the pumps, is realized by means of a mechanical contact point after the mating of the gears teeth. Then the pressure difference between the two regions, where the discharge region is generally referred to as higher pressure region and the suction as lower pressure region, does the rest.

Internal Gear Pumps work very similar to the EGP. Referring to Fig. 19 the internal gear is the driving one and is mate with the prime mover. Its rotation transmits motion to the idle (external) gear. Fluid enters on the suction side of the pump and flows into the cavities between the rotor and the idler. While rotating the gears teeth cyclically mate. As the gears begin to mesh the fluid is forced out of the cavities and is discharged from the pump. Here cavitation happens when the fluid pocket trapped in the space of the mating opens to the suction side. Basically, the working principle is approximately the same for EGP or IGP. From this is intuitive to understand that the handling of the contact point in a CFD simulation is fundamental in order to achieve ultimate reliable results. Different techniques have been employed in various codes in order to achieve a successful simulation, but the handling of the contact point still remains a bottle neck for the majority of commercial codes. The main technique generally employed depends on the inner algorithm upon which the chosen software is based, so that each programme implies a different strategy. The main technique is represented by the *Remeshing Technique* (or Dynamic approach) which is based upon a rotation/substitution/interpolation approach. In this strategy a routine, that can be already implemented in the software (as for PumpLinx) or customized by the user (as in ANSYS), regulates the remeshing of the fluid region based upon the cells quality due to the deformation it undergoes during the movement of the gears. The remeshing can also depend upon a previous defined time in which the mesh is known to maintain a good quality of the cells. In any case, since these pumps have cyclic repetitions, so the definition of a sub-cycle routine is enough for all the simulation. Obviously this approach, being automated or custom defined requires little time steps, for both the high velocities for which these machines work and the necessity to minimize the deformation of cells. Anyway, no limits exist to the fantasy of the user. Another meshing method that is implemented in Star-CCM+ code only is the Overset Mesh method. This method relies on an Activation/Deactivation strategy, where the overset meshes (if required more than one) selectively deactivate the background mesh (involving the total rotational fluid region) cells once they intersect the same space. This technique is theoretically the only one that permits to handle a zero contact point between all the native commercial softwares strategies. Its potency was demonstrated in works such as the one of Muzzioli et al. [58] where the good agreement of a robust realistic physic simulation along with the correct handling of the contact point produces high reliable results for gear pumps. For the next articles review, when PumpLinx is used, where not differently specified the cavitation model to be considered is the *Singhal*.

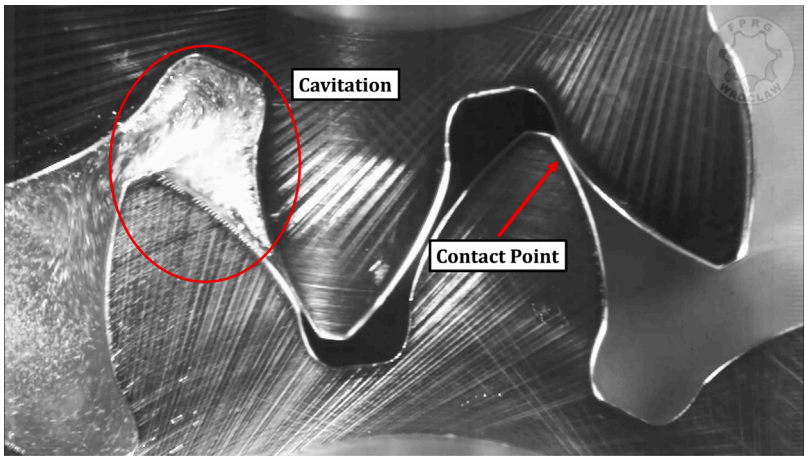

Fig. 18. Cavitation phenomenon in an EGP (Wroclaw).

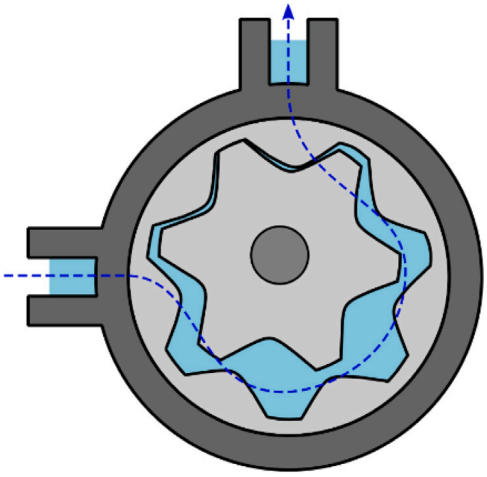

Fig. 19. Generic working scheme for a Gerotor Pump.

5.1. Operating conditions

Starting with parametric studies based on the variation of the operating conditions (being the simplest to investigate), Jiang et al. [59] studied the cavitation phenomenon in a gerotor pump with variable rotational speeds, with a 5 μm leakage gaps and a *Singhal* model. The authors found out that at 5000 rpm cavitation becomes relevant and at 6000 rpm it spreads throughout the inlet port and into the pockets on the inside trace of the crescent island. Also, the reducing in performance at 5000 rpm is in good agreement with the experimental results and validates the effect of the cavitation of flow rate efficiency. Ruvalcaba et al. [60] analysed a gerotor pump performance under various conditions and found out the influence of cavitation and leakage flow, but no cavitation model is explained. The simulation was carried over in FLUENT environment. The results showed that cavitation itself does not impact much on the performance of gerotor pumps. Leakage flow, then, specifically the one occurring in tip-to-tip clearance, was shown to have critical impact on flow deficiency demonstrated by the excellent agreement with the experimental data. Del Campo [61], based on their work from 2012 [62], brought forth a 2D analysis in FLUENT environment of an EGP and compared the results with particle image tracking obtained via experimental analysis. The authors studied the influence of a loss inlet factor (i.e. inlet pressure below atmospheric pressure) and of an high outlet pressure. The effects of cavitation registered at low pressure tend to disappear with high working pressure (with a 100 bar jump) while inlet flow and pressure ripples, volume of air evolution and cavitation cloud characteristics seem not to be particularly affected while cavitating jet at the backlash clearance may be suppressed at high pressure. High pressure also strongly reduces volumetric ratio due to the disappearing of the virtual contact point created by the cavitation cloud in proximity of the disengaging between the teeth moving to the inlet. The inlet pressure effects then were studied for 1500 and 3000 rpm. On cavitation the reduced pressure increased the inlet water hammer pulsations and grew with the increasing of air generated via cavitation. Along with the increasing velocity the cavitation clouds extended in the domain with a three times increasing of air. These clouds got trapped in the inter-teeth volume and were transported towards the impulsion chamber. These effects with the addition of the uniformity of the flow at high velocities showed that only at high enough velocities air is transported to the pressure side through the interteeth volumes, so that only in similar cases cavitation really shows a bad impact on the pump performances. Zhou et al. [63] studied by means of ANSYS FLUENT an helical gear pump with high speeds and high pressures. They employed a remeshing algorithm and the *Singhal* cavitation model. The authors reported the impact of cavitation on the mean maximum pressure and the negative pressure in the system for 10 000 and 12 000 rpm, and found out that since cavitation itself is a phenomenon which happens at low pressures the impact on the maximum pressure was found to be not so relevant if compared with a case with non cavitating condition. The values at the end of the cycle were found to be generally higher than the case where no cavitation happened. In the case of the negative pressure cavitation stabilized around a value that was much higher than the case with no cavitation. Casari et al. [64] studied the effect of cavitation in an ORC cycle and implemented the dynamic of regulation of the system. Three different conditions were studied in the case of cavitation occurrence, namely 450 rpm and 293 K, then 450 rpm and 294.5 K and finally 475 rpm and 294.5 K. Basically the first condition represents the standard, the second represents an outlet temperature increase, the third is the compensation operated by the system. It was found that with the increasing in temperature (acting on the saturation pressure of the fluid) and rotational speed the cavitation resulted in an increased production of vapour. Li et al. [65] studied the influence of different rotational speeds and different suction pressures on the cavitation in an EGP. Since no model is effectively cited but only a reference is done to the *Rayleigh–Plesset* equation, we can suppose that it was implemented to support the cavitation prediction. The impact was registered in terms of volume fraction of vapour distribution in the fluid domain and in terms of maximum volume fraction of vapour. As expected the increasing in rotational speed led to an increase in both distribution and values of the vapour volume fraction while the opposite happened with the increasing in pressure suction. Interestingly the formation of

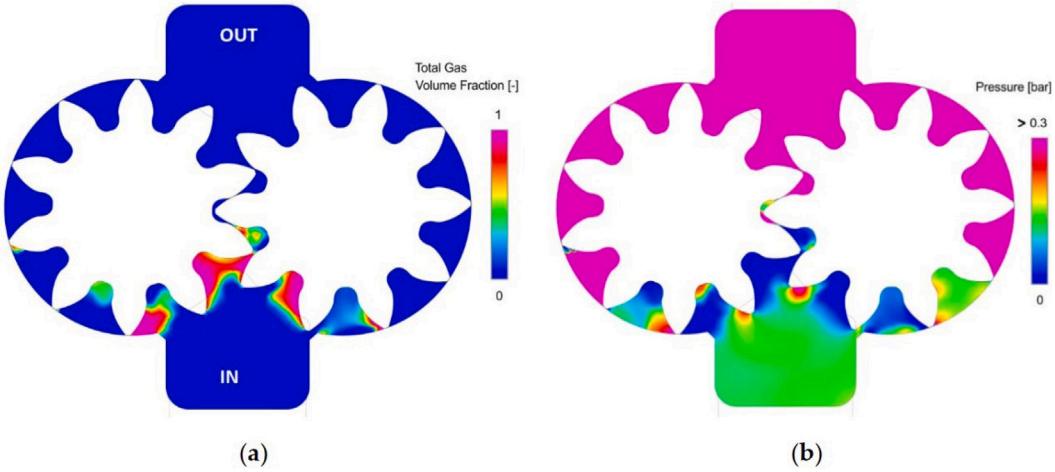

Fig. 20. Simulated total gas volume fraction (a) and pressure field (b) at 2000 rpm in Corvaglia et al. [66].

vapour clouds happened in correspondence to the last driven tooth in correspondence to the casing on the inlet side.

Corvaglia et al. [66] evaluated the impact of tooth space pressure in case of incomplete filling. The authors reported a fall of the flow rate when lower pressure values were reached, denoting a condition of incomplete filling of the tooth spaces. This, considering the low working pressure values, led to the conclusion of the effect mainly being due to the incomplete filling in SimericsMP+. For their simulation the authors employed the Equilibrium Dissolved Gas model, that does not consider the dynamics of release and dissolution of the air. In this model the mixture density is calculated as function of the mass fraction of vapour and gas (air). The fraction of dissolved/undissolved gas is determined by the Henry's law then. The obtained contours revealed that air was not only released in proximity of the gears meshing but also in the isolated tooth chambers due to the centrifugal force that pushes outward the oil as shown in Fig. 20.

5.2. Design modifications

Heisler et al. [67] examined the effect of various housing, thrust plate and gear designs for an external gear pump with means of PumpLinx software. With increasing rotational velocity cavitation was found to increase, due to the fewer time that the fluid has at its disposal to flow out of the trapped volume to the suction. Then, considering that cavitation mainly occurs in proximity to gears after disengaging, the authors modified the teeth so that slots were realized in order to force the fluid in the trapped volume. It was found the important effect of slots in eliminating vapour formation in close proximity to their position, with the best result corresponding to a 2% decrease in vapour volume fraction. Finally the authors proposed a modification of the external leakages (since internal leakages are substantially not modifiable) by means of an orifice in which the pressure of the exiting fluid is equal to that of the inlet, this leading to suppressing the formation of vapour. Optimum performances occurred for an exiting fluid pressure of 1000psi. Hsieh [68] studied a gerotor pump with different span angles. Along with an increase in area efficiency with the increasing of the span angle (20°, 30° and 40°), both the outlet pressure, the outflow rate and velocity increased leading to a correspondent increase in the vapour volume fraction.

Hao et al. [69] (see Fig. 21) studied a new rotor profile derived from the replacement of a coefficient in the original ellipse equations. They showed that such a modification resulted in the same vapour fraction at low speed while at high speeds (4000 rpm) the values are slightly higher for the new profile, this suggesting that cavitation itself in not particularly influenced by such modifications. Sedri et al. [70] analysed the effect of new compression slots applied on the gears. The scope

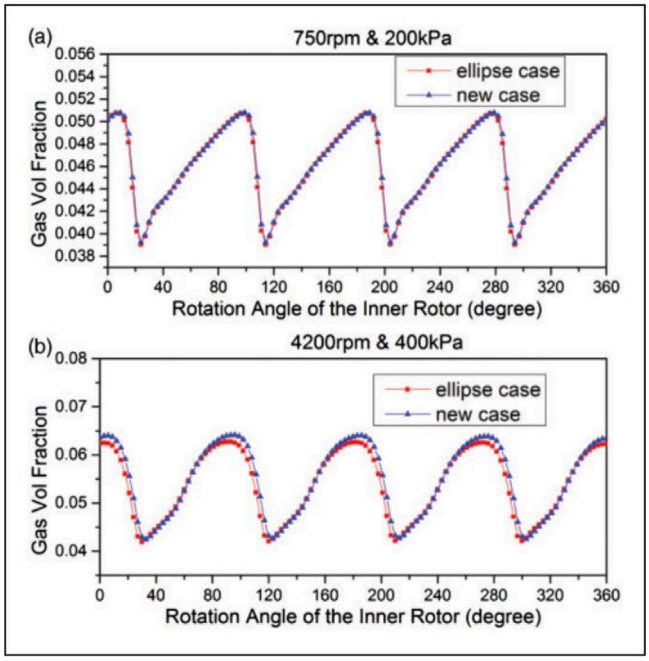

Fig. 21. Gas volume fraction between rotors in Hao et al. [69].

of these decompression slots (also known as relief grooves) is to have an optional method to discharge the high pressure fluid contained in the central shrinking cavities to the discharge zone. Also, they serve to facilitate the expansion cavities to refill with fluid and to present pressure drop leading to cavitation in the intake region. The authors proposed, differently by Heisler [71], to create two shallow slots on each side of the gears in order to prevent the inevitable flowing into the cavities that connect each tooth. In this study the authors showed that for a rotational speed of 506 rpm the cavitation occurrence was suppressed effectively by the addition of the decompression slots, also the pressure pulsations decreased significantly so that pump operations became smoother.

5.3. Contact point and leakages

Del Campo et al. [62] simulated a 2D external gear pump with FLUENT, and were able to simulate a virtual contact point by means of

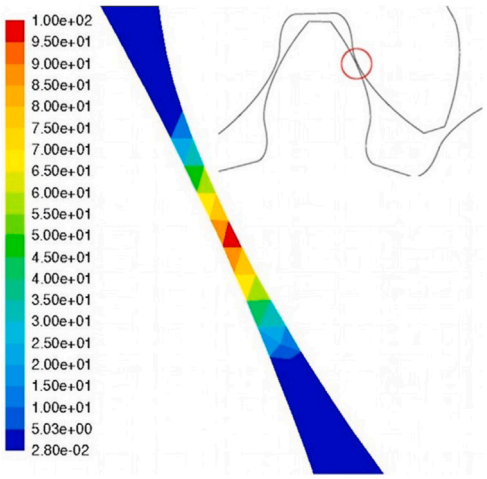

Fig. 22. Dynamic viscosity imposed in the contact point position in Del Campo et al. [62].

an UDF, where a local condition of high viscosity, as in Fig. 22 was set in order to prevent the flowing of fluid through the meshing leakages.

The authors then proceeded to two multi-phase simulations with *S-S* cavitation model and *ZGB* in the other, with different rotational velocities and two different liquids, water and oil respectively. Apart from the inability of the 2D models to predict the volumetric efficiency, the analysis showed the interesting phenomenon for which the higher the pump speed the shorter the time for cavitation clouds to dissipate before another cavitation mechanism could start, therefore this enhances the air volume stability. Then, another interesting result was the formation of an amount of air at the backlash clearance between the gears, in order to fill the increasing volume next to the contact point, and this cloud acted as a second contact point blocking the backward oil flow and increasing the outlet flow rate. Frosina et al. [72] studied an high pressure EGP taking in account for all leakages in the model with PumpLinx. The authors also dedicated to the calculus of the gap and shift angle in order to reproduce at best a resemblance of the contact between the teeth (see Fig. 23).

The results reported by the authors are perfectly in line with the general findings, where the generated vapour fraction, located in correspondence to the volumes enclosure by the teeth, once engaged starts to expand (or to open) towards the suction, as for the dependency upon the rotational velocity of the cavitation intensity. In addition the cavitation extension inside the enclosed fluid package demonstrated that if not properly simulated, a virtual contact point leads to an unrealistic inner expansion of the vapour fraction. Mocilan et al. [73] proposed a 3D model in ANSYS, where by means of an ideal sealing at teeth engagement isolated the volume in between the pump discharge and suction. To do so, the ideal sealing was realized with a total of 30 meshes dynamically uploaded after a precise number of degrees of rotation. The cavitation found by employing a cavitation model (not clearly specified) resulted in a not so intense cavitation but it was correctly found in the suction side once the teeth disengaged. Zhao et al. [74] made a simulation of a continuous contact helical gear with means of Simeric-MP+ and the use of a Mismatched Grid Interface in order to realize a dynamic mesh, then the model so realized was confronted with a previous lumped parameter simulation. The authors simulated two different cases with different rotational speed, pressure and lateral gap thickness. The first simulation at 50 bar and 1000 rpm was the only with the existence of the sealing surface with a gap length of 0 μm. The authors showed an interesting comparison if simulating a more realistic simulation with means of a sealing surface with a simulation where small gaps exist in between the teeth where they should engage. This leakages in high pressure conditions led to high compressibility effects that resulted in a choking condition of the fluid, with a sudden decrease of the sonic velocity of the operating fluid immediately after the gap to 10 m/s. This effect depended mainly on the large pressure drop at the tiny gap with the simultaneously increasing of the volume, which introduced a further de-pressurizing effect, so that the rapid decrease in pressure in the downstream chamber provoked cavitation which decreased the fluid sound speed.

5.4. Others

Dufresne et al. [75] attempted to simulate a 2D fully coupled model for an external gear pump, with means of Fluid Structure Interaction and fully adaptive and steer method for meshing. Herein the cavitation phenomena appear as drastic pressure drops of pressure with the increasing rotational speed, which leads to the formation and immediate implosion of cavities is also related to pinion's cracking. For that last reason the FSI analysis was conducted in order to find the zone of major stress during the working of the pump.

Frosina et al. [76] analysed the variable displacement pump of the lubrication oil circuit of an high performance engine with PumpLinx implementing a *Singhal* cavitation model in the software. The authors found out that the risks zone are found in some vanes in the suction area. The most problematic operating conditions in terms of cavitation phenomenon were found to be those characterized by high speed rotations. In this study no further analysis was conducted on the cavitation phenomenon if not the mentioning of its use. In the end, this study proved the reliability of CFD codes to simulate EGP proving them to be a solid method.

Ghazanfarian et al. [77] studied a double external gear pump 2D configuration with various rpm and pressure outlet with OpenFOAM. While focusing mainly on other fluid-dynamic aspects the cavitation model was used to determine in which region vapour volume is generated at 4000 rpm. The authors found out that two regions exist where cavitation occurs and that those are placed between two contacting teeth near the respectively suction chambers, as was effectively expected. Labaj et al. [78] focused on the application of a *S-S* model on a 3D model of an External Gear Pump with means of a dynamic mesh, with inlet pressure of 0.1 MPa and outlet pressure of 25 MPa and a rotational speed 3000 rpm. They found a weak cavitation with 0.5 value of the vapour volume fraction for this pump but the authors were able to address the responsibility of cavitation as one of the causes of the torque surges and the pressure surges size. Altare [79] did not directly show the effects of cavitation of a lubricating pump at 5000 rpm but found out that in order to fulfil a correct simulation for a working pump and to correctly reproduce the physical behaviour the implementation of a cavitation model is mandatory, being a characteristic of volumetric pumps at particular high working conditions.

In their 2019 work Milani et al. [80] analysed a gerotor pump with a double inlet (see Fig. 24). The authors investigated the performance variation based on the progressive realistic physic implementation in the Star-CCM+ environment. Doing so the authors investigated the influence of real fluid properties on the simulation accuracy. Four total cases were investigated, the incompressible, compressible, thermal field implementation and finally cavitation/aeration phenomena models implementation. For the last simulation the *R-P* equation model was enabled in the software. The IGP was in this case approximated with a constant lateral leakage between the gears and the case. Then the overset mesh method was used to simulate the gears teeth mating. The overset mesh was generated along the perimeter of the internal gear. Since a zero contact point exists the zero-overset gap mesh is required to handle the mating point. The authors found that the implementation of more realistic physic conditions leads to more accurate results, in particular the variable density and viscosity led to an error on the experimental data of less than 2%. When comes to cavitation/aeration phenomena the occurring was investigated in the operating conditions that were set to 33 bar and 3300 rpm. Within this conditions no aeration was detected and only a small percentage of oil vapour was detected close to the internal gear profile.

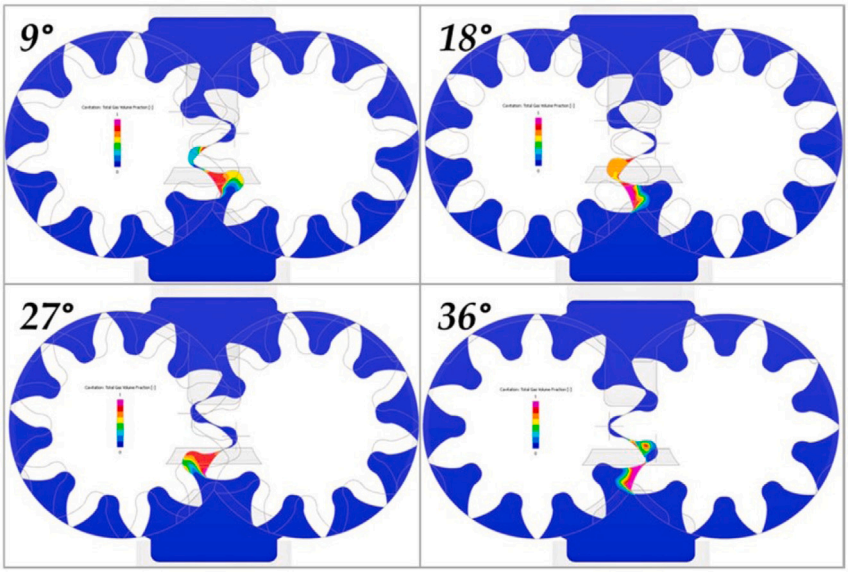

Fig. 23. Distribution of the total gas fraction in a section view of the pump at 250 bar, 2500 rpm for different rotation angles in Frosina et al. [72].

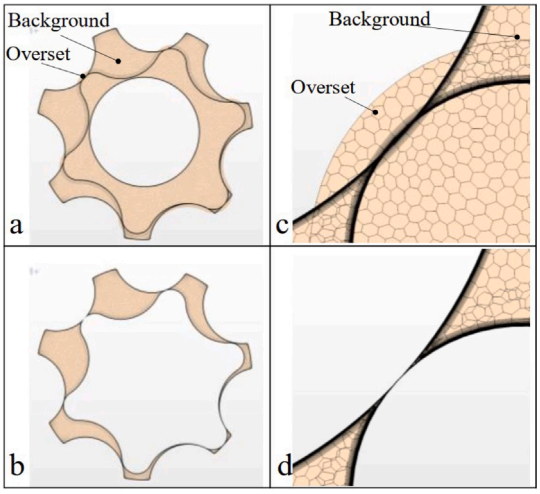

(a)

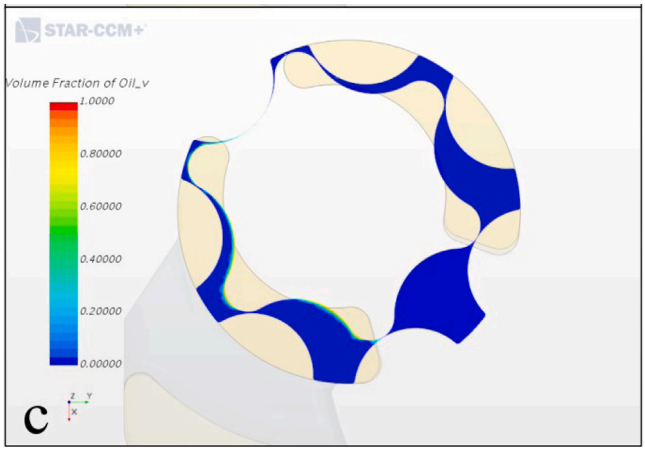

(b)

Fig. 24. (a) Overset mesh (b) Oil cavitation in Milani et al. [80].

6. Mixed flow pumps

The mixed flow pumps are a peculiar centrifugal pump type with the addition of a mixed flow impeller. When the impeller rotates, the action of the liquid is both centrifugal force and axial thrust and the liquid is inclined to flow out of the impeller. This kind of pump is fundamentally an in between to a centrifugal and an axial flow pump. These pumps cover the transition range between radial flow pumps and axial flow pumps, since they combine both the centrifugal force and the propeller action of the impeller's vanes, which leads to a relatively large discharge pressure and an high amount of elaborated flow. Since the working principle is partly identical to the centrifugal pumps the analysis methodology is extremely similar to that applied to centrifugal pumps. The rotating region is in fact separated but interfaced to the stationary region and often the multiple reference frame is used.

6.1. Operating conditions

In order to produce an affordable design aimed to maximize the cavitation performance, Bonaiuti et al. [81] carried over the parametric study of a water-jet pump system. A *R-P* model for the bubble dynamics was chosen in ANSYS CFX environment. With means of CFD analysis the final design was calibrated in order to detect cavitation, and the experimental test and the simulations were conducted with a partial mass flow rate (M/M_{des} = 0.86) and an inlet total pressure equal to 80% of the operating value. With a comparison between contours of the vapour volume fraction was enlightened that in design conditions the overall working regime is cavitation-free. Then in partial working conditions a trapezoidal-shaped attached cavitation region takes place on the lower part of the blade suction side, with also some degree of cavitation on the blade shroud (see Fig. 25).

Kerschberger et al. [82] studied an high-speed pump-turbine and characterized the cavitation inception by means of the cavitation number and ANSYS CFX software. For this study, the rotating parts mesh was generated using the ASTROE software, while ICEM CFD was used for the tubes meshes. In order to evaluate the cavitation phenomenon the authors used a statistical histogram evaluation of the pressure field. Then, with means of the Thoma cavitation coefficient (i.e. cavitation number) the potential cavitation given by the pressure distribution was estimated. In pump mode, cavitation and instabilities limited the head-capacity curve, while in turbine mode vortices in the draft tube were linked to the pressure fluctuations determined smooth operations.

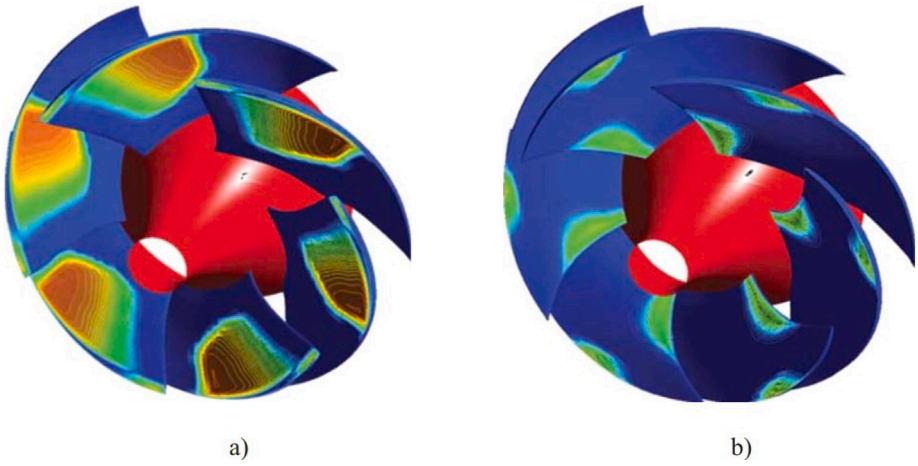

Fig. 25. Visualization of vapour volume fraction contours on the blade surface for (a) the baseline and (b) for the final design in Bonaiuti et al. [81].

The results showed a feasible accuracy of the CFD prediction onto the experimental results. Singh et al. [83] made use of the *R-P* model to investigate the cavitation in a Pump-Turbine model at operating conditions of partial, normal and excessive loading for both pump and turbine mode. The authors found out that the results where different for the different modes of the machine. In the pump operative mode the highest air volume fraction was found at partial load while the other two load conditions showed similar values distribution. For the turbine operative mode then, the higher values of air volume fraction were found at normal and excessive loading but with way smaller values than those of the pump mode. Xia et al. [84] analysed by means of a *ZGB* model a high-speed waterjet propulsion pump under three operating conditions, at design, small and large flow rate with different decreasing values of the NPSHa. At design flow rate the low pressure regions in both the pressure and suction side have a correspondent cavitation region which air volume fraction increases with the decreasing of the NPSHa, with the suction side reaching a stage of developed cavitation where the phenomenon will block the entire impeller passage in the worst areas even leading to cavitation happening on the pressure side of the blade. In the pressure side the cavitation remains confined to more restricted areas near the internal edges of the blade. The analysis of the partial conditions show a similar trend at the suction side for the cavitation development, with the similar grow from the inside to the outside of the blade of the vapour volume fraction. The case for large flow rates (or also in waterjet propulsion pump mode) shows instead a different variation tendency, where in the transition of the NPSHa from 1.9 to 1.45 the cavitation develops from the hub to the rim of the blade. Then pressure becomes higher than the vapour pressure so that cavitation is suppressed. Then lowering further the NPSHa leads to an hard cavitation with bubbles blocking the passage of the impeller. In this case the critical NPSHa and cavitation area result to be bigger than for the other conditions. Xu et al. [85] analysed the transient characteristics of a mixed-flow pump under different cavitation conditions. The authors point out that under cavitation conditions the critical NPSH increases as the tip clearance increases with deterioration of cavitation performance. Also, in the impellers with tip clearance the cavitation bubbles tend to attach to the blade suction side and the attachment length increases as the tip clearance increases. The use of different tip leakages showed that confronted to the zero tip leakage the cavitation shows an apparent attached area in the impeller tip clearance region. Below the NPSHc values of each pump the existence of tip clearances lead to fully developed cavitation condition, also this leads to the leakage between suction side and pressure side where the high speed flow through the clearance leads to a low pressure in the tip clearance. The connection phenomenon reaches its maximum for the lowest value of NPSHa reported where the bubbly region in the different passages are all in connection and the area increases as the tip clearance enlarges.

6.2. Design modifications

Zhao et al. [86] studied a pump-sump within a single-intake rectangular sump with means of the *Full Cavitation model (Singhal)* available in ANSYS CFX. ANSYS ICEM CFD was used for the mesh generation. The pump was analysed with and without the addition of an anti-vortex device (AVD), so that a common solution could be verified in its efficacy. Results proved that with the addition of an AVD the vortices that tend to form in the pump intake near the side and the rear wall were suppressed. Then, plotting the vorticity distribution in flow and channel width directions (for different positions) the authors demonstrated that even if not absent the presence of an AVD reduces the maximum vorticity value. Finally, in the cavitation analysis NPSH plot and vapour volume fraction distribution on the blades surfaces were reported and linked. As the NPSH reduces the surface cavitation region expands and eventually leads to serious blockage of the flow. Hao et al. [87] investigated a pump as turbine mixed-flow pump. In order to improve the existent model of *ZBG* in ANSYS CFX the authors decided not to use a constant for the p_v term, since it varies according to pressure fluctuations. So an improved vapour pressure was implemented as $p_v = p_{sat} + 0.195\rho_m\kappa$, where ρ_m is the weighted density of vapour and liquid, p_{sat} is the saturation pressure and κ the turbulent kinetic energy (see Fig. 26).

The authors investigated the effect of different tip clearances and found out that the addition of tip leakages worsens the cavitation performance, and the radial force increases with cavitation deterioration, also its direction changes with the cavitation deterioration due to the asymmetrical distribution of cavitation region. Kim et al. 2019 [88] studied the effect of various blade thickness on the cavitation characteristics. At the design-point was found that with the increasing of the blade thickness a decrease in the annular flow passage is obtained, resulting in an higher flow velocity which corresponds a smaller pressure for the flow rate remaining the same. With the blade thickness increasing, the amount of vapour increases for each $NPSH_{re}$, which is defined as the point with a 3% reduction compared with the total head without cavitation, and the bubbles distribution has a direct correlation with flow separation and acts as a blockage to reduce the performance of the pump. Finally, depending on the blade thickness the authors found that the bubbles distribution presents distinctly different shapes at the same inlet pressure. Zhao et al. [89] studied the control of blade cavitation by means of passive control by obstacles, that is depending on inflow non-uniformities and unsteadiness due to modifications operated on the blades surface, in origin intended to block the re-entrant jet to depress the cloud cavitation. With the simulations have been reported the efficiency of the obstacles to slow the advancement of cavitation development, but turbulent wake cavitation is introduced by the obstacles.

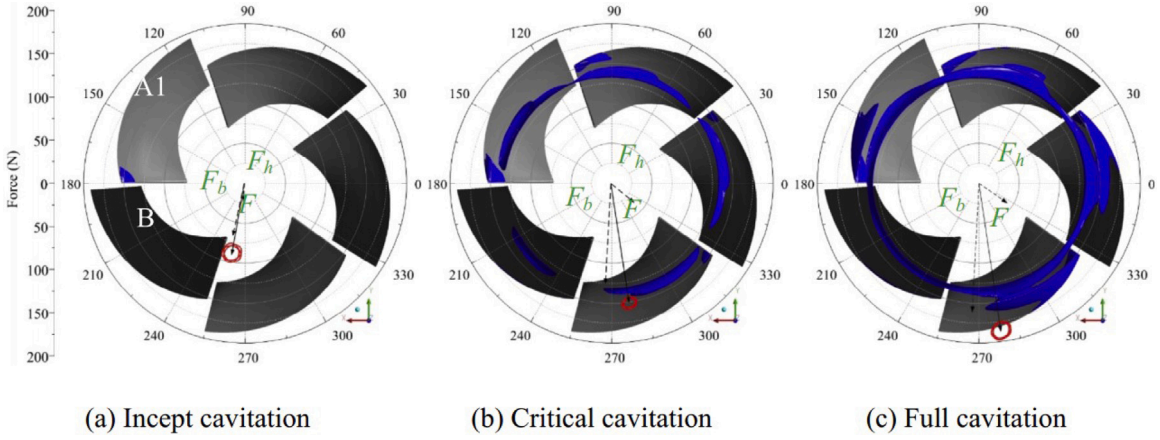

Fig. 26. Cavitation region and radial force orbit for a specified tip clearance in Hao et al. [87].

6.3. Detailed fluid dynamics analyses

Focusing on the evolution of vortices Huang et al. [90] investigated the cavitation development in a mixed-flow water-jet pump, also considering the single contribution of the terms of the vorticity transport equation. It was found, as for example stressed out in many axial flow pumps papers reported above, that cavitation enhances vortex generation and flow unsteadiness. Vortices were also found to be located at the cavity interface, especially the downstream one. Then, vortex dilatation and baroclinic torque were found to dramatically increase at the cavity interface and the vortex dilatation term shown a larger magnitude than the baroclinic torque. Xu et al. [48] simulated cavitating turbulent flows in an axial water-jet pump with a particular focus on the vorticity characterization with means of a *ZGB*. In order to sufficiently simulate the vortices the SAS turbulence model was used, so that the ability to resolve the unsteady turbulent structures is enhanced compared to a RANS model but is not as expensive as for a LES model. Then, to visualize the different vortex structures various techniques have been implemented and compared. In this study the tip leakage cavitation extends from the pressure to the suction side in the blade tip region and gradually develops downstream along the blade, while sheet cavitation interacts with the tip leakage vorticity cloud cavitation that makes the vortices to be extremely unstable. With a particular focus on the tip leakage cavitation was found that it enhances the turbulent kinetic energy in the unstable vortex cavitation region and the downstream lip leakage vortex region along the blade. Cavitation also affects the relative axial velocity in the region of the tip leakage cavitation. Kim et al. [91] correlated the head drop and unsteady bubble pattern to cavitation in the case of a mixed-flow pump with different incidence angle, namely type A which has a narrower inlet diameter and the type B which has a larger incident angle. The study was operated varying the cavitation number and using the *R-P* model for the cavitation implementation. In first place the bubbles are generated from the suction surface of the impeller leakage edge with the decreasing of pressure. Then analysing the impact of the incidence angle the authors found that in the region where the single bubble is generated by cavitation the component of circumferential velocity is mainly distributed, so that the incidence angle affects this velocity component and has a proportional effect (see Fig. 27).

Considering the type A, which can be defined as a pump with a relatively good suction performance exhibits a uniform vapour distribution, but in the case of type B, so with a poor suction performance, obtains a non-uniform vapour distribution. The subsequent effect is that a uniform distribution leads to a faster head drop and inverse for the non-uniform distribution. Shi et al. [92] studied the effect of cavitation on the energy conversion characteristics of a multiphase with a *ZGB* model. The main correlation herein studied were the effects of cavitation on pressure loading, output power and pressurization performance. It was demonstrated that with the decrease of the cavitation number (and correspondingly with the increase of cavitation) the pressure loading decreases for the same span. For the output power of the pump, considering the two contributions of moment generated by the pressure on the impeller surface and the viscous moment generated by the impeller with no slip wall, is firstly found that the pressure term is the main contribution and the overall power decreases with the increase of cavitation. With a particular attention to the impeller domains it can be seen that with the decrease of the cavitation number the distribution of power inverts from the highest cavitation number to the smallest. In general is found that in both static and dynamic pressure power condition the power decreases accordingly to the cavitation number. Regarding the pressurization performance, considering the two main losses being the turbulent and the friction loss, the authors found out that with the evolution of cavitation the turbulent dissipation loss in the impeller domain decreases gradually. In facts in the inception and critical cavitation conditions the flow is mainly turbulent but in critical and fracture stages the increment in the friction loss is larger, so that the overall loss increment strongly increases. In the inception and critical cavitation stages the intensity of cavitation is weak as it appears at the leading edge of suction side and the impact on performances is weak. Then the cavitation is strengthen in critical and fracture cavitation. In the last two cavitation stages performance severely deteriorates and results by two aspects, the first being the output power generated by viscous and pressure load that reduces at critical fraction cavitation and fracture cavitation stage, while the second being the flow loss generated by friction that enlarges greatly due to the increase of dynamic pressure power and back flow vortex resulted from large adverse pressure gradient.

7. Results and discussion

7.1. Cavitation and pumps

In the analysed papers a lot of different topics were cover on the cavitation phenomenon in pumps. Focusing on the phenomenon of the cavitation itself the reported literature permits to define which are the main factors that affect cavitation and its rising in pumps. Together to the main trigger effect being a sudden and localized pressure drop, various other boundary phenomena help enhancing the cavitation inception. Considering the distancing from the design point the most simple of all is the decrease in the pressure at the inlet, that logically shifts the pump from operating at the design point to a lower point, where this effect was found affecting both the centrifugal/axial pumps and the gear pumps. By the other hand also the overload working condition of a pump leads to the increase in the phenomenon of cavitation. For the mixed flow pumps, based on the discovered literature, the

Fig. 27. Vapour volume fractions results for the higher cavitation number in Kim et al. [91].

overload and partial load conditions were found to give different results on cavitation depending on the operational mode, if pump or turbine, of the machine. For external gear pumps this is easily demonstrated by the rotation velocity, where the higher the rotation and the worse is the cavitation. The structure integrity of the machine is also another important factor, where eventual imperfections can lead to higher nucleation sites that enhance the formation of bubbles, or the walls roughness that with higher levels promotes cavitation and increases the vapour volume fraction. This obviously holds well for each machine typology. Few works also investigated the role of the working fluid itself, where for example diesel was compared to water in a centrifugal pump with diesel leading to higher cavitation areas but less vapour volume fractions. In the case of axial flow pumps the role of sandy water was investigated and the presence of sediment particles was found to enhance cavitation in a positive mutual influence. Inherently the design of the machine itself, the single components strongly affect the probability of the whole machine to be more or less prone to the inception of cavitation. For pumps characterized by the presence of an impeller and a stator the main design parameters where found to be

- The tip leakage between the impeller's blades and the casing, where the bigger the leakage the higher the cavitation phenomenon becomes.
- The shape of the blade tips, where the less curve and most sharp the shape the worse.
- The blade attack angles, where positive values where demonstrated to improve cavitation performances in axial flow pumps but in centrifugal pumps the incipient positions seemed to remain the same.
- The number of blades, where more the blades the higher the cavitation.
- The blade thickness, where at its amount corresponds a decrease in the annular flow with a decrease in the pressure leading to an increase in the vapour volume fraction.

For the external gear pumps then the main factor relies on the engaging between the teeth of the two gears, since this is an unavoidable working principle. Here all the design modifications were generally tested in order to improve the reliability of the pump and so to lower the cavitation inception. The modifications were generally related to the profile of the teeth or peculiar modification in order to reduce the high pressures in the temporary closed volumes, and so lower the pressure drop once disclosing to the inlet side.

Only inherently the centrifugal/axial pumps a lot of research was performed inherently the characterization and evolution of cavitation. For both the types of pumps the strong relationship between turbulence and cavitation was found out. For centrifugal pumps the relative vortex stretching was found to enlarge the cavity and subsequently enhance cavitation in [23]. For axial flow pumps a major quantities of papers focusing on the role of the vortex structures were found. Here the primer role of the tip leakage vortex (TLV) was extensively stressed out [41,42,47,48,51,53,54,93]. Another peculiar vortex structure, namely the suction side perpendicular cavitating vortex (SSPCV), was investigated in [52]. The results showed that also between these vortex structures and cavitation a mutual link exists where one enhances the other. The main principle that seems to govern this mutual interaction is the pressure fluctuation that adds instabilities to the flow which are beneficial for the promotions of the precedents. Specifically regarding this kind of analyses, is obvious that the standard formulation of the cavitation models is not enough precise to capture all this dynamic behaviours, mainly due to the simplification in the truncation of the second order terms that generally link the most complex dynamics in the vapour-liquid interfaces. Also, improved turbulence models are often employed since the resolution of the vortex structures is mainly dependent on the turbulence model. Easier formulation may regard the simple use of more advanced methods, such as the detached eddy simulation DES in [55] that works as a halfway between RANS and LES turbulence models. Also, the simple modification of a single term in the turbulence model as can be the case for the eddy viscosity term in [54] with the use of a filter-based density correction model (FBDCM) or the same in a RNG turbulence model with a filter-based model in [51]. An other option is the modification of a cavitation model in order to take in count the bubble-bubble interaction as done in [23]. For the characterization of the vortex structures other methods were also employed specifically focusing on the vortex structures individuation, as in the case of the boundary vorticity flux implemented in [50].

7.2. Summaries

In Table 1 a summary is reported based on the cavitation model in use. Here in the central column the most frequent analyses typology is reported followed on the last column by the number of papers where their use was mentioned. The *R-P* model results to be the least employed, with its use limited to parametric kind of analyses, coupled with a wear model and for cavitation evolution characterization (these last two limited to one paper each). The most used is the *ZGB*, where the range of applications varies from the parametric analyses to the detailed study of the evolution of cavitation. Then the *Singhal* model follows. These two models, as it can be verified by Table 1, are the most used when cavitation modelling is mandatory. A part from the complexity of these models, the reason seems to depend mainly on their implementation in ANSYS (for *ZGB*) and PumpLinx (for *Singhal*) softwares. For centrifugal pumps indeed the use of ANSYS environment is the most common choice, while for EGP the choice generally falls on PumpLinx. The *S-S* model in the end results to be the last one in terms of use. Even if of slight lesser use, the *SS* cavitation model gets its implementation in the vast majority of analyses kind, spanning from the usual parametric study to the cavitation evolution and contact point modelling too. The reason behind this vast application may reside in its simplest formulation if compared to the *ZGB* and *Singhal*, but no particular motivations are found generally in the papers upon the model of use, so that remains an hypothesis. It is also interesting to point out that, even if Debarpan [35] evidenced that no particular difference is appreciable in the produced results, the simpler formulation seems to be the main motivation for its avoiding in the most

Table 1
Cavitation models summary.

Model	Analysis	Papers
Rayleigh - Plesset	Parametric + Wear Model + Cavitation Evolution	9
Singhal	Cavitation Evolution + Comparisons + Parametric + Contact Point Modelling	13
Zwart–Gerber–Belamri	Cavitation Evolution + Parametric + Comparison + Contact Point Modelling + Model Improvement + Wear Model	25
Schnerr–Sauer	Cavitation Evolution + Models Improvement + Parametric + Comparison + Contact Point Modelling	11

Table 2
Machine kind summary.

Machine	Cavitation models	Mesh technique	Total papers
CP	*R-P(1) - Singhal(2) - ZGB(10) - S-S(6)*	Frozen-Transient Rotor interfaces	24
AFP	*R-P*(3) - *ZGB*(10) - *Singhal*(2) - *S-S*(2)	Frozen-Transient Rotor interfaces/Moving Sliding Methodology	19
EGP	*R-P(2) - Singhal(7) - ZGB(2) - S-S(3)*	Dynamic/Moving-Sliding Methodology/Overset Method	21
MFP	*R-P(3) - Singhal(2) - ZGB(3)*	Mixing Plane/Frozen-Transient Rotor interfaces	13

of the parametric cases. Then, if an analysis is to be carried out with an higher precision and detail the use of more complex models is mandatory of course, since they take in account for more complex physics phenomena. Obviously even the *ZGB* and the *Singhal* models have been proved to lack some superior precision for specific analyses. Also, each model suffers the same weakness in the truncation to the second order terms, neglecting then peculiar dynamics that are specific of the vapour-liquid interfaces.

Within Table 1 a general overview based on the cavitation models was given. In Table 2 then the summary is shifted to the singular machines kind. In this way it is possible to link the models not only to the kind of pumps but also to the peculiar meshing techniques that have been developed in the years for the different pumps working mechanisms. In the first line relative to centrifugal pumps the predominance of the use of the *ZGB* is evident, and that leads to the vast use of ANSYS in the CFD analyses, as aforementioned in the relative paragraph above. In ANSYS, being it FLUENT or CFX, the physic domain is divided into two distinct kind of regions, the static ones and the rotating ones. These regions are then linked to each other by means of the *Frozen* (if the relative motion is static as for the static rotor) or the *Transient* (if transient, or characterized by a moving element, as the name suggests as in the case of the impeller) interfaces. Then the movement of the rotating parts can be operated with various techniques, where the most common is the Multiple Reference Frame. Here a new rotating reference frame is generated united with the rotating part. Generally, the frozen rotor interface is more often mentioned than the transient interface in the various analysed papers.

Inherently the axial flow pumps, the predominant use of the *ZGB* cavitation model is evident as per the centrifugal flow pumps. The same way the mesh techniques employed are basically the same, thus regarding the general use of the frozen/transient interface for the data exchange between the computational region and the multiple reference frame for the relative motion of the impeller. Even if ANSYS is logically the prevalent choice in most of the discovered works few appear to made use of different codes. Such is the case as Gong et al. [53] that made use of Star-CCM+ and for Li et al. [94] with Pumplinx.

Switching to the EGP the predominance of the *Singhal* method derives from its implementation in PumpLinx software, which is widely the most used software when the analyses of gear pumps is performed. When using PumpLinx the system rotation is managed all internally and automatically by the software. Here the single rotating meshes generated along the gears are matched with the Moving-Sliding methodology. When ANSYS is employed then the meshing method is generically referred to as Dynamic or Re-meshing. For this kind of methodology the movement of the mesh, which is generated all along the gears and comprises the gears chamber in its entirety, is managed by an external code (User Defined Function) that has to be previously compiled by the user himself. During the rotation the mesh is continuously stretched and/or compressed and is substituted after a fixed number of time steps due to the proximity of structural integrity limits of the cells. This leads obviously to requiring more computational time but it reserves some new possibilities like the handling of the contact point that is avoided in PumpLinx. Few works need to be mentioned, as they depart from the others softwares generally in use. Dufresne [75] made use of the commercial code ADINA which made use of a technique named Steering Mesh approach, which basically is a remeshing method. Then Ghazanfarian et al. [77] in OpenFOAM implemented a remeshing approach. Another recent approach that the author was able to find in [58,80] is the Overset Methodology implemented in Star-CCM+, where the re-meshing is substituted with a continuous activation/deactivation of the cells between a fixed background mesh and one or more overset rotating mesh. The capability of this technique of handling the generation and disappear of zero contact points makes it a promising technique to push further such simulations for higher physic reliable results.

Finally, for the mixed flow pumps the use of the different models do not show a clear preference for one or the other between the considered models. It is more interesting to note, strictly to the cavitation models that the *S-S* model was not found by the present authors to be employed in this kind of machines analyses. While within ANSYS the mesh technique is the same as for the centrifugal/axial flow pumps, in few works [81,82] the Mixing Plane approach was used, but then quickly discarded for the well known frozen/transient rotor interface.

7.3. Conclusions

In the present paper an overview on the cavitation modelling within pump machines with means of CFD was presented. First of all, the main numerical methods where reported, and the basic demonstration was carried forth, so that the main assumptions behind the single method could be highlighted. This was intended to give the necessary comprehension of the physic implemented in each models, so that goals and limits of the code can be understood and related to the obtained results. This is also why a *Schnerr–Sauer* could be expected to give less precise results if compared to a *Zwart–Gerber–Belamri*, relating to its intrinsic complexity. Obviously, more detailed analyses should be

carried on to emphasize the differences between the methods at a digital code level, which is not the objective of this work. The main conclusions that were highlighted in this review are

- The cavitation and pumps subsection of the results reports the main factors affecting the cavitation insurgence in pumps as they are analysed through the CFD methods. A part from the inlet pressure factor that affects all the pumps kind herein reported, each typology has its own specific peculiar factors. For EGP the main critical point is the zero contact between the gear teeth and the design studies were mainly focused on this. For the CP/AP/MP the list of factors is wider and include various design parameters which the most are focused on the impeller characteristics. The relation between turbulence and cavitation was also investigated for these similar pumps typologies and led to the highlighting of the mutual positive influence between the vortices structures and cavitation.
- As results from Table 2 Centrifugal Pumps are the main studied machines when it comes to cavitation in CFD simulations. Gear Pumps follow immediately, where EGP are the main focus of this analyses with some studies on IGP that follow. Axial Flow Pumps result in a related bibliography slightly inferior to that of EGP, even with its strong similarities to CP. Mixed Flow Pumps then are a rising field of interest in the CFD analysis of pumps and in the last years are gaining more studies within the cavitation phenomenon.
- The most used cavitation models applied to this topic comprehend the *Schnerr–Sauer*, the *Zwart–Gerber–Belamri* and the *Singhal* models. Inherently to CP and AP the *ZGB* model is the most common choice, while in EGP/IGP the *Singhal* model is the most used. In MFP then no particular preference of use was detected based on the considered works.
- The choice of use for the cavitation model mainly depends on the employed code. ANSYS CFX and FLUENT are the most common choices regarding CP/AP and the *ZGB* is a native model developed by ANSYS engineers themselves, so it comes obvious to find an high prevalence on the use of this cavitation model when analysing the relative studies. For Gear Pumps the choice for the software falls mostly on PumpLinx and herein the *Singhal* cavitation model seems to be the preferred choice, where considering the introductory work by Ding et al. [94] the explicit employing of this cavitation model is a built in choice of the software developers. Being so the state of the art, it can be determined that ANSYS code gives the best results and is more capable to adapt to CP and similar machines. PumpLinx then was effectively developed specifically to treat Gear Pumps so the frequency results in the use of the code are not surprising and confirm this trend.
- As pointed out previously, the code's frequency of use of the cavitation models is arbitrary and often is not justified on the model itself. For example, the fact that the *S-S* model can be able to produce more reliable results is in contrast with the lesser use of it in favour of more complex models.
- In between of all the analysed works, when it comes to CFD simulations and cavitation phenomena parametric studies are the most common above all. Centrifugal and Axial pumps then were chose mostly when detailed analyses on the cavitation evolution or improvements of the existing cavitation models had to be performed. This trend probably depends on the ease of simulating such machines. Obviously peculiar works as the customization of codes to handle peculiar physics as the zero contact point are specific of Gear Pumps machines. It is important to point out that lot of works have been found to not include any cavitation model and to rely only to the NPSH values. Even if this technique gains satisfactory results it must be pointed out that does not permit to obtain precise and detailed results on the cavitation phenomenon. Only the use of cavitation models enables the numeric system to approach realistic and reliable results in term of CFD physic fields.
- Each cavitation model is inefficient when a strong reliability on the realistic simulation of cavitation is required, specifically for the most critic operating conditions. This because each of the models, even the most complex *Singhal - Full Cavitation Model*, truncates the second order terms.
- The meshing methodology depends exclusively on few factors: the code of choice and the typology of the analysed machine. For CP/AP the methodology is comprised of the definition of two regions, static and rotating, and the use of an effective rotation, if transitory, or a Multiple Reference Frame, if stationary. For Gear Pumps the general methodology is the Dynamic/Remeshing approach, where a sub-routine of a fixed number of meshes are defined and cyclically substituted for a fixed number of rotation steps. Specifically to commercial codes PumpLinx makes use of the Moving-Sliding method that internally manages the remeshing based on the communication between the intersecting cells. Few works exist at the moment with the use of Star-CCM+ but the Overset methodology, entirely based on the activation and deactivation of the intersecting cells seems to be a promising technique to be employed since it seems to be the only capable of handling the zero contact point. When different authors tried to handle the zero contact point different strategies were implemented, mainly based on ANSYS and Remeshing techniques with external codes.

Declaration of competing interest

The authors declare that they have no known competing financial interests or personal relationships that could have appeared to influence the work reported in this paper.

Data availability

No data was used for the research described in the article.

References

[1] Ansys software, 2022, URL: https://www.ansys.com/.
[2] PumpLinx software, 2022, URL: https://www.simerics.com/pumplinx/.
[3] W.F. Noh, P. Woodward, SLIC (Simple line iinterface calculation), in: Proc. 5th Int. Conf. Fluid Dyn. Lect. Notes Physics, Vol. 59, 1976, pp. 330–340, URL: https://www.ptonline.com/articles/how-to-get-better-mfi-results.
[4] C.W. Hirt, B.D. Nichols, Volume of Fluid (VOF) method for the dynamics of free boundaries, J. Comput. Phys. 39 (1981) 201–225, http://dx.doi.org/10.1016/0021-9991(81)90145-5.
[5] O. Lord Rayleigh, On the Pressure Developed in a Liquid During the Collapse of a Spherical Cavity, Vol. 34, No. 200, Taylor & Francis, 1917, pp. 94–98, http://dx.doi.org/10.1080/14786440808635681, URL: https://www.tandfonline.com/doi/abs/10.1080/14786440808635681.
[6] M.S. Plesset, The dynamics of cavitation bubbles, J. Appl. Mech. Trans. ASME 16 (3) (1949) 277–282, http://dx.doi.org/10.1115/1.4009975.
[7] G.H. Schnerr, J. Sauer, Unsteady cavitating flow - A new cavitation model based on a modified front capturing method and bubble dynamics, in: Proceedings of FEDSM'00, Vol. 251, No. January 2000, ASME, 2000, pp. 1073–1079.
[8] G. Schnerr, J. Sauer, Development of a new cavitation model based on bubble dynamics, ZAMM Z. Angew. Math. Mech. (2001) 561–562.
[9] G. Schnerr, J. Sauer, Physical and numerical modeling of unsteady, in: 4th International Conference on Multiphase Flow, No. May 2001, ICMF, 2001, pp. 1–12.
[10] D. Spalding, A method for computing steady and unsteady flows possessing discontinuities of density, CHAM Rep. 910 (2) (1974).
[11] P.J. Zwart, A.G. Gerber, T. Belamri, A two-phase flow model for predicting cavitation dynamics, in: 5th International Conference on Multiphase Flow, Vol. 152, No. January 2004, 2004, p. 152.
[12] A.K. Singhal, M.M. Athavale, H. Li, Y. Jiang, Mathematical basis and validation of the full cavitation model, J. Fluids Eng. 124 (3) (2002-09) 617–624, http://dx.doi.org/10.1115/1.1486223, URL: https://asmedigitalcollection.asme.org/fluidsengineering/article/124/3/617/444321/Mathematical-Basis-and-Validation-of-the-Full.
[13] M. Alexis, F. Visser, Cavitation effects in centrifugal pumps-A review, Binama Maxime. Int. J. Eng. Res. Appl. 6 (5) (2016) 52–63.

[14] X. Li, S. Yuan, Z. Pan, J. Yuan, Y. Fu, Numerical simulation of leading edge cavitation within the whole flow passage of a centrifugal pump, Sci. China Technol. Sci. 56 (9) (2013) 2156–2162, http://dx.doi.org/10.1007/s11431-013-5311-5.

[15] H.L. Liu, D.X. Liu, Y. Wang, X.F. Wu, J. Wang, Application of modified k-ω model to predicting cavitating flow in centrifugal pump, Water. Sci. Eng. 6 (3) (2013) 331–339, http://dx.doi.org/10.3882/j.issn.1674-2370.2013.03.009.

[16] A.U. Rehman, S. Shinde, V.K. Singh, A.R. Paul, A. Jain, R. Mishra, CFD based condition monitoring of centrifugal pump, in: Proceedings of COMADEM 2013 - Helsinki, No. June 2013, 2013, pp. 1–6.

[17] T. Lei, Z.B. Shan, C.S. Liang, W.Y. Chuan, W.B. Bin, Numerical simulation of unsteady cavitation flow in a centrifugal pump at off-design conditions, Proc. Inst. Mech. Eng. C 228 (11) (2014) 1994–2006, http://dx.doi.org/10.1177/0954406213514573.

[18] R. Tao, R. Xiao, F. Wang, W. Liu, Cavitation behavior study in the pump mode of a reversible pump-turbine, Renew. Energy 125 (2018) 655–667, http://dx.doi.org/10.1016/j.renene.2018.02.114.

[19] Y. Ye, X. Zhu, F. Lai, G. Li, Application of the semi-analytical cavitation model to flows in a centrifugal pump, Int. Commun. Heat Mass Transfer 86 (June) (2017) 92–100, http://dx.doi.org/10.1016/j.icheatmasstransfer.2017.04.021.

[20] B. Cui, J. Chen, Visual experiment and numerical simulation of cavitation instability in a high-speed inducer, Proc. Inst. Mech. Eng. A 234 (4) (2020) 470–480, http://dx.doi.org/10.1177/0957650919867173.

[21] V. Lomakin, O. Bibik, Numerical prediction of the gas content effect on the cavitation characteristics of the pump using the simplified Rayleigh-Plesset equation, IOP Conf. Ser. Mater. Sci. Eng. 492 (1) (2019) 0–8, http://dx.doi.org/10.1088/1757-899X/492/1/012037.

[22] J. Pei, M.K. Osman, W. Wang, J. Yuan, T. Yin, D. Appiah, Unsteady flow characteristics and cavitation prediction in the double-suction centrifugal pump using a novel approach, Proc. Inst. Mech. Eng. A 234 (3) (2020) 283–299, http://dx.doi.org/10.1177/0957650919863636.

[23] W. Sun, L. Tan, Cavitation-vortex-pressure fluctuation interaction in a centrifugal pump using bubble rotation modified cavitation model under partial load, Trans. ASME, J. Fluids Eng. 142 (5) (2020) 1–11, http://dx.doi.org/10.1115/1.4045615.

[24] H. Li, F.J. Kelecy, A. Egelja-maruszewski, S.A. Vasquez, Advanced computational modeling of steady and unsteady cavitating flows, in: Proceedings of IMECE2008, ASME, 2008, pp. 1–11.

[25] R. S. Muttalli, S. Agrawal, H. Warudkar, CFD simulation of centrifugal pump impeller using ANSYS-CFX, Int. J. Innov. Res. Sci. Eng. Technol. 03 (08) (2014) 15553–15561, http://dx.doi.org/10.15680/ijirset.2014.0308066.

[26] H.L. Liu, J. Wang, Y. Wang, H. Zhang, H. Huang, Influence of the empirical coefficients of cavitation model on predicting cavitating flow in the centrifugal pump, Int. J. Nav. Archit. Ocean Eng. 6 (1) (2014) 119–131, http://dx.doi.org/10.2478/IJNAOE-2013-0167.

[27] W. Sanchez Ocana, C. Carvajal, J. Poalacin, M.I. Pazmino, E.S. Jacome, L. Basantes, Cavitation analysis with CFD techniques of the impeller of a centrifugal pump, Indian J. Sci. Technol. 11 (22) (2018) 1–6, http://dx.doi.org/10.17485/ijst/2018/v11i20/123055.

[28] Q. Hu, Y. Yang, W. Cao, Computational analysis of cavitation at the tongue of the volute of a centrifugal pump at overload conditions, Adv. Prod. Eng. Manag. 15 (3) (2020) 295–306, http://dx.doi.org/10.14743/apem2020.3.366.

[29] Q.X. Hu, Y. Yang, W.D. Shi, Cavitation simulation of centrifugal pump with different inlet attack angles, Int. J. Simul. Model. 19 (2) (2020) 279–290, http://dx.doi.org/10.2507/IJSIMM19-2-516.

[30] W. Xu, X. He, X. Hou, Z. Huang, W. Wang, Influence of wall roughness on cavitation performance of centrifugal pump, J. Braz. Soc. Mech. Sci. Eng. 43 (6) (2021) 1–12, http://dx.doi.org/10.1007/s40430-021-03023-3.

[31] D. Zhu, R. Xiao, W. Liu, Influence of leading-edge cavitation on impeller blade axial force in the pump mode of reversible pump-turbine, Renew. Energy 163 (2021) 939–949, http://dx.doi.org/10.1016/j.renene.2020.09.002.

[32] S.F. Xie, Y. Wang, Z.C. Liu, Z.T. Zhu, C. Ning, L.F. Zhao, Optimization of centrifugal pump cavitation performance based on CFD, IOP Conf. Ser. Mater. Sci. Eng. 72 (Forum 3) (2015) http://dx.doi.org/10.1088/1757-899X/72/3/032023.

[33] A.R. Al-Obaidi, Monitoring the performance of centrifugal pump under single-phase and cavitation condition: A CFD analysis of the number of impeller blades, J. Appl. Fluid Mech. 12 (2) (2019) 445–459, http://dx.doi.org/10.29252/jafm.12.02.29303.

[34] S.S. Deng, G.D. Li, J.F. Guan, X.C. Chen, L.X. Liu, Numerical study of cavitation in centrifugal pump conveying different liquid materials, Results Phys. 12 (February) (2019) 1834–1839, http://dx.doi.org/10.1016/j.rinp.2019.02.009.

[35] D. Paul, H. Agarwal, B.R. Ponangi, CFD analysis of two-phase cavitating flow in a centrifugal pump with an inducer, Heat Transf. 49 (6) (2020) 3854–3881, http://dx.doi.org/10.1002/htj.21812.

[36] N. Fecser, I. Lakatos, Cavitation measurement in a centrifugal pump, Acta Polytech. Hung. 18 (4) (2021) 63–77, http://dx.doi.org/10.12700/APH.18.4.2021.4.4.

[37] H.S. Shim, K.Y. Kim, Effects of the cross-sectional area of a volute on suction recirculation and cavitation in a centrifugal pump, Trans. ASME, J. Fluids Eng. 142 (5) (2020) 1–14, http://dx.doi.org/10.1115/1.4045573.

[38] S. Xi, Z. Desheng, X. Bin, J. Yongxin, S. Weidong, B.P. van Esch, Experimental investigation of the transient patterns and pressure evolution of tip leakage vortex and induced-vortices cavitation in an axial flow pump, Trans. ASME, J. Fluids Eng. 142 (10) (2020) 1–11, http://dx.doi.org/10.1115/1.4047529.

[39] H. Ding, F.C. Visser, Y. Jiang, M. Furmanczyk, Demonstration and validation of a 3D CFD simulation tool predicting pump performance and cavitation for industrial applications, Trans. ASME, J. Fluids Eng. 133 (1) (2011) 1–14, http://dx.doi.org/10.1115/1.4003196.

[40] K. Hosono, Y. Kajie, S. Saito, K. Miyagawa, Study on cavitation influence for pump head in an axial flow pump, J. Phys. Conf. Ser. 656 (1) (2015) http://dx.doi.org/10.1088/1742-6596/656/1/012062.

[41] L. Shi, D. Zhang, Y. Jin, W. Shi, B.P. Van Esch, A study on tip leakage vortex dynamics and cavitation in axial-flow pump, Fluid Dyn. Res. 49 (3) (2017) http://dx.doi.org/10.1088/1873-7005/aa6637.

[42] X. Shen, D. Zhang, B. Xu, C. Ye, W. Shi, Experimental and numerical investigation of tip leakage vortex cavitation in an axial flow pump under design and off-design conditions, Proc. Inst. Mech. Eng. A 235 (1) (2021) 70–80, http://dx.doi.org/10.1177/0957650920906295.

[43] W.G. Li, Verifying performance of axial-flow pump impeller with low NPSHr by using CFD, Eng. Comput. (Swansea, Wales) 28 (5) (2011) 557–577, http://dx.doi.org/10.1108/02644401111141019.

[44] L. Cao, S. Watanabe, S. Momosaki, T. Imanishi, A. Furukawa, Low speed design of rear rotor in contra-rotating axial flow pump, Int. J. Fluid Mach. Syst. 6 (2) (2013) 105–112, http://dx.doi.org/10.5293/IJFMS.2013.6.2.105.

[45] W. Feng, Q. Cheng, Z. Guo, Z. Qian, Simulation of cavitation performance of an axial flow pump with inlet guide vanes, Adv. Mech. Eng. 8 (6) (2016) 1–8, http://dx.doi.org/10.1177/1687814016651583.

[46] P. Lin, M. Liu, W. Zhao, Z. Liu, Y. Wu, F. Xue, Y. Zhang, Influence of tip clearance on the performance of a screw axial-flow pump, Adv. Mech. Eng. 9 (6) (2017) 1–10, http://dx.doi.org/10.1177/1687814017704357.

[47] L. Shi, D.S. Zhang, R.J. Zhao, W.D. Shi, Y.X. Jin, Effect of blade tip geometry on tip leakage vortex dynamics and cavitation pattern in axial-flow pump, Sci. China Technol. Sci. 60 (10) (2017) 1480–1493, http://dx.doi.org/10.1007/s11431-017-9046-9.

[48] S. Xu, X. ping Long, B. Ji, G. bin Li, T. Song, Vortex dynamic characteristics of unsteady tip clearance cavitation in a waterjet pump determined with different vortex identification methods, J. Mech. Sci. Technol. 33 (12) (2019) 5901–5912, http://dx.doi.org/10.1007/s12206-019-1135-y.

[49] S. Saito, M. Shibata, H. Fukae, E. Outa, Computational cavitation flows at inception and light stages on an axial-flow pump blade and in a cage-guided control valve, J. Therm. Sci. 16 (4) (2007) 337–345, http://dx.doi.org/10.1007/s11630-007-0337-2.

[50] R. Zhang, H.X. Chen, Numerical analysis of cavitation within slanted axial-flow pump, J. Hydrodyn. 25 (5) (2013) 663–672, http://dx.doi.org/10.1016/S1001-6058(13)60411-4.

[51] D. Zhang, L. Shi, R. Zhao, W. Shi, Q. Pan, B.P. van Esch, Study on unsteady tip leakage vortex cavitation in an axial-flow pump using an improved filter-based model, J. Mech. Sci. Technol. 31 (2) (2017) 659–667, http://dx.doi.org/10.1007/s12206-017-0118-0.

[52] L. Wang, F. Tang, Y. Chen, H. Liu, Evolution characteristics of suction-side-perpendicular cavitating vortex in axial flow pump under low flow condition, J. Mar. Sci. Eng. 9 (10) (2021) http://dx.doi.org/10.3390/jmse9101058.

[53] J. Gong, W. zhen Luo, T. cheng Wu, Z. yuan Zhang, Numerical analysis of vortex and cavitation dynamics of an axial-flow pump, Eng. Appl. Comput. Fluid Mech. 16 (1) (2022) 1921–1938, http://dx.doi.org/10.1080/19942060.2022.2122570.

[54] H. Feng, Y. Wan, Z. Fan, Numerical investigation of turbulent cavitating flow in an axial flow pump using a new transport-based model, J. Mech. Sci. Technol. 34 (2) (2020) 745–756, http://dx.doi.org/10.1007/s12206-020-0121-8.

[55] S. Xi, Z. Desheng, X. Bin, S. Weidong, B.P. (Bart) van Esch, Experimental and numerical investigation on the effect of tip leakage vortex induced cavitating flow on pressure fluctuation in an axial flow pump, Renew. Energy 163 (2021) 1195–1209, http://dx.doi.org/10.1016/j.renene.2020.09.004.

[56] P. Lin, D. Hu, Z.J. Lin, M.Q. Liu, C.L. Tang, S. Wang, The mechanism of joint effects of axial-flow pump cavitation and sediment wear, Adv. Mech. Eng. 12 (5) (2020) 1–14, http://dx.doi.org/10.1177/1687814020923066.

[57] P. Lin, D. Hu, J.M. Lu, S. Wang, CFD numerical simulation of sand-contained cavitation characteristics of axial-flow pump, Adv. Mech. Eng. 13 (7) (2021) 1–14, http://dx.doi.org/10.1177/16878140211032785.

[58] G. Muzzioli, L. Montorsi, A. Polito, A. Lucchi, A. Sassi, M. Milani, About the influence of eco-friendly fluids on the performance of an external gear pump, Energies 14 (4) (2021-02) http://dx.doi.org/10.3390/en14040799.

[59] Y. Jiang, M. Furmanczyk, S. Lowry, D. Zhang, C.Y. Perng, A three-dimensional design tool for crescent oil pumps, SAE Tech. Pap. (724) (2008) http://dx.doi.org/10.4271/2008-01-0003.

[60] M.A. Ruvalcaba, X. Hu, Imece2011-62226 Gerotor fuel pump performance and leakage study, in: Proceedings of the ASME 2011 International Mechanical Engineering Congress & Exposition, ASME, 2011, pp. 1–9.

[61] D. Del Campo, R. Castilla, G.A. Raush, P.J. Gamez-Montero, E. Codina, Pressure effects on the performance of external gear pumps under cavitation, Proc. Inst. Mech. Eng. C 228 (16) (2014) 2925–2937, http://dx.doi.org/10.1177/0954406214522990.

[62] D. Del Campo, R. Castilla, G.A. Raush, P.J. Gamez Montero, E. Codina, Numerical analysis of external gear pumps including cavitation, Trans. ASME, J. Fluids Eng. 134 (8) (2012) 1–12, http://dx.doi.org/10.1115/1.4007106.
[63] Y. Zhou, L. Wu, M. Hao, Three-dimensional numerical analysis of an operating helical rotor pump at high speeds and high pressures including cavitation, MATEC Web Conf. 114 (2017) 0–5, http://dx.doi.org/10.1051/matecconf/201711404005.
[64] N. Casari, E. Fadiga, M. Pinelli, S. Randi, A. Suman, Pressure pulsation and cavitation phenomena in a micro-ORC system, Energies 12 (11) (2019-06) http://dx.doi.org/10.3390/en12112186.
[65] M.-x. Li, G.-l. Yang, G.-x. Bai, Dynamic simulation research on cavitation in internal multiconnected volumes gear pump, in: The 8th International Conference on Fluid Power and Mechatronic, IEEE, 2019.
[66] A. Corvaglia, M. Rundo, P. Casoli, A. Lettini, Evaluation of tooth space pressure and incomplete filling in external gear pumps by means of three-dimensional CFD simulations, Energies 14 (1) (2021) http://dx.doi.org/10.3390/en14020342.
[67] A.S. Heisler, J.J. Moskwa, F.J. Fronczak, The design of low-inertia, high-speed external gear pump/motors for hydrostatic dynamometer systems, SAE Tech. Pap. (2009) http://dx.doi.org/10.4271/2009-01-1117.
[68] C.F. Hsieh, Fluid and dynamics analyses of a gerotor pump using various span angle designs, Trans. ASME, J. Mech. Des. 134 (12) (2012) 1–13, http://dx.doi.org/10.1115/1.4007703.
[69] C. Hao, Y. Wenming, L. Guangming, Design of gerotor oil pump with new rotor profile for improving performance, Proc. Inst. Mech. Eng. C 230 (4) (2016) 592–601, http://dx.doi.org/10.1177/0954406215618228.
[70] F. Sedri, A. Riasi, Investigation of leakage within an external gear pump with new decompression slots: numerical and experimental study, J. Braz. Soc. Mech. Sci. Eng. 41 (5) (2019-05) http://dx.doi.org/10.1007/s40430-019-1717-8.
[71] A.S. Heisler, J.J. Moskwa, F.J. Fronczak, A.F. Guo, T.T. Jiang, T. Wang, Y.P. Hu, D.J. Zhang, Simulated helical gear pump analysis using a new CFD approach, Appl. Mech. Mater. 556–562 (2009) 1–11, URL: http://www.scopus.com/inward/record.url?eid=2-s2.0-84902103435&partnerID=tZOtx3y1.
[72] E. Frosina, A. Senatore, M. Rigosi, Study of a high-pressure external gear pump with a computational fluid dynamic modeling approach, Energies 10 (8) (2017-07) http://dx.doi.org/10.3390/en10081113.
[73] M. Mocilan, S. Husár, J. Labaj, M. Zmindák, Non-stationary CFD simulation of a gear pump, Procedia Eng. 177 (2017) 532–539, http://dx.doi.org/10.1016/j.proeng.2017.02.257.
[74] X. Zhao, A. Vacca, S. Dhar, Lumped-parameter and a 3D CFD approach of simulation, in: Proceedings of the BATH/ASME 2018 Symposium on Fluid Power and Motion Control, ASME, 2018, pp. 1–11.
[75] M. Dufresne, Fluid structure interaction studies for experimental validations of plastic external gear pump, in: An International Conference on Applications of Fluid Engineering, 2012, pp. 1–6.
[76] E. Frosina, A. Senatore, D. Buono, M. Olivetti, A tridimensional CFD analysis of the oil pump of an high performance engine, SAE Tech. Pap. 1 (2014) http://dx.doi.org/10.4271/2014-01-1712.
[77] J. Ghazanfarian, D. Ghanbari, Computational fluid dynamics investigation of turbulent flow inside a rotary double external gear pump, Trans. ASME, J. Fluids Eng. 137 (2) (2015) 1–8, http://dx.doi.org/10.1115/1.4028186.
[78] J. Labaj, S. Husar, Analysis of gear pump designed for manufacturing processes, Appl. Mech. Mater. 803 (2015) 163–172, http://dx.doi.org/10.4028/www.scientific.net/amm.803.163.
[79] G. Altare, M. Rundo, Computational fluid dynamics analysis of gerotor lubricating pumps at high-speed: Geometric features influencing the filling capability, Trans. ASME, J. Fluids Eng. 138 (11) (2016) http://dx.doi.org/10.1115/1.4033675.
[80] M. Milani, L. Montorsi, S. Terzi, G. Storchi, R. Emilia, Approach accounting for the fluid compressibility and temperature, in: Proceedings of the ASME 2019 International Mechanical Engineering Congress and Exposition, ASME, 2019, pp. 1–10.
[81] D. Bonaiuti, M. Zangeneh, R. Aartojarvi, J. Eriksson, Parametric design of a waterjet pump by means of inverse design, CFD calculations and experimental analyses, Trans. ASME, J. Fluids Eng. 132 (3) (2010) 0311041–03110415, http://dx.doi.org/10.1115/1.4001005.
[82] P. Kerschberger, A. Gehrer, Hydraulic development of high specific-speed pump-turbines by means of an inverse design method, numerical flow-simulation (CFD) and model testing, IOP Conf. Ser. Earth Environ. Sci. 12 (2010) 012039, http://dx.doi.org/10.1088/1755-1315/12/1/012039.
[83] P.M. Singh, C. Chen, Z. Chen, Y.-D. Choi, Cavitation characteristics of a pump-turbine model by CFD analysis, KSFM J. Fluid Mach. 18 (4) (2015) 49–55, http://dx.doi.org/10.5293/kfma.2015.18.4.049.
[84] C.Z. Xia, L. Cheng, Y.N. Shang, J.R. Zhou, F. Yang, Y. Jin, Numerical simulation on the cavitation of waterjet propulsion pump, IOP Conf. Ser. Mater. Sci. Eng. 129 (1) (2016) http://dx.doi.org/10.1088/1757-899X/129/1/012011.
[85] Y. Xu, L. Tan, Y. Liu, S. Cao, Pressure fluctuation and flow pattern of a mixed-flow pump with different blade tip clearances under cavitation condition, Adv. Mech. Eng. 9 (4) (2017) 1–12, http://dx.doi.org/10.1177/1687814017696227.
[86] Y.X. Zhao, C.G. Kim, Y.H. Lee, CFD study on flow characteristics of pump sump and performance analysis of the mixed flow pump, IOP Conf. Ser. Mater. Sci. Eng. 52 (TOPIC 7) (2013) http://dx.doi.org/10.1088/1757-899X/52/7/072006.
[87] Y. Hao, L. Tan, Symmetrical and unsymmetrical tip clearances on cavitation performance and radial force of a mixed flow pump as turbine at pump mode, Renew. Energy 127 (2018) 368–376, http://dx.doi.org/10.1016/j.renene.2018.04.072.
[88] Y.I. Kim, S. Kim, H.M. Yang, K.Y. Lee, Y.S. Choi, Analysis of internal flow and cavitation characteristics for a mixed-flow pump with various blade thickness effects, J. Mech. Sci. Technol. 33 (7) (2019) 3333–3344, http://dx.doi.org/10.1007/s12206-019-0628-z.
[89] G. Zhao, L. Cao, B. Che, R. Wu, S. Yang, D. Wu, Towards the control of blade cavitation in a waterjet pump with inlet guide vanes: Passive control by obstacles, Ocean Eng. 231 (January) (2021) 108820, http://dx.doi.org/10.1016/j.oceaneng.2021.108820.
[90] R. Huang, B. Ji, X. Luo, Z. Zhai, J. Zhou, Numerical investigation of cavitation-vortex interaction in a mixed-flow waterjet pump, J. Mech. Sci. Technol. 29 (9) (2015) 3707–3716, http://dx.doi.org/10.1007/s12206-015-0816-4.
[91] Y.I. Kim, H.M. Yang, J.W. Suh, S. Kim, K.Y. Lee, Y.S. Choi, Numerical study on the cavitation phenomenon for the head drop and unsteady bubble patterns with a difference in the incidence angle of a mixed-flow pump, Adv. Mech. Eng. 12 (4) (2020) 1–18, http://dx.doi.org/10.1177/1687814020914790.
[92] G. Shi, S. Wang, Y. Xiao, Z. Liu, H. Li, X. Liu, Effect of cavitation on energy conversion characteristics of a multiphase pump, Renew. Energy 177 (2021) 1308–1320, http://dx.doi.org/10.1016/j.renene.2021.05.119.
[93] S. Xi, Z. Desheng, X. Bin, S. Weidong, B.P. (Bart) van Esch, Experimental and numerical investigation on the effect of tip leakage vortex induced cavitating flow on pressure fluctuation in an axial flow pump, Renew. Energy 163 (2021) 1195–1209, http://dx.doi.org/10.1016/j.renene.2020.09.004.
[94] H. Ding, F. Visser, Y. Jiang, M. Furmaczyk, Predicting pump performance and cavitation for industrial applications, in: Proceedings of the ASME 2009 Fluids Engineering Division Summer Meeting Proceedings of FEDSM2009, ASME, 2009, pp. 1–17.